Ionization and quenching of excited atoms with the production of fast electrons

N. B. Kolokolov and A. B. Blagoev

St. Petersburg University, Sofia University

(Submitted 23 September 1992; revised 25 November 1992)
Usp. Fiz. Nauk **163**, 55–77 (March 1993)

Studies of reactions involving excited atoms, which result in the release of electrons with energies exceeding the mean plasma electron energy, are reviewed. Particular attention is devoted to plasma electron spectroscopy (PES) which combines the advantages of studies of elementary plasma processes with those of traditional electron spectroscopy. Data obtained by investigating the following reactions are reported: chemoionization with the participation of two excited inert-gas atoms, Penning ionization of atoms and molecules by metastable helium atoms, and electron quenching of excited inert-gas atoms and mercury atoms. The effect of processes in which fast electrons are emitted on plasma properties is discussed.

INTRODUCTION

Excited and, especially, metastable states of atoms and molecules play an important part in plasma processes. Indeed, the excited-particle concentrations in plasma can exceed the charged-particle concentration by an order of magnitude or more, so that the potential energy stored in excited states can in such cases exceed the kinetic energy of the electron gas by a substantial factor. It is then important to bear in mind the high chemical activity of the excited states and their effective participation in ionization, dissociation, and excitation processes.

Collisions between slow heavy particles that result in the emission of electrons and ions are of particular interest from the standpoint of both numerous practical applications and theoretical interpretation. They are the so-called chemoionization processes in which one or more of the colliding particles are in an excited state. To emphasize their importance, we recall Penning lasers in which inversion is achieved by chemoionization. Moreover, chemoionization may be one of the stages in the establishment of an inverted population as a result of transitions in a readily-ionized impurity. In particular, in powerful high-pressure infrared lasers using a mixture of helium and heavy-gas impurities, the ionization process relies on charge transfers on helium ions or on chemoionization.

Chemoionization is also used as an important stage in the laser separation of isotopes and the detection of impurities.

There is an extensive literature on chemoionization reactions (see, for example, Refs. 1–5). However, reactions involving two excited particles have until recently remained relatively ignored, and studies of the energy spectrum of electrons emitted in these reactions have been lacking because such experiments are difficult to perform.

When chemoionization occurs in plasma, the ratio of the energy of emitted electrons to the mean energy of plasma electrons is a significant parameter. When fast, hot electrons are thus emitted, a nonequilibrium state is produced and affects excitation, ionization, and recombination processes, the diffusion of charged particles, and the temperature of the main electron group.

Quenching by electron impact plays an important part in changes in the concentration of excited and, especially, metastable particles. It is involved together with chemoionization in charged-particle reactions and the transfer of excitation energy to electrons. It is clear that studies of quenching processes are a source of information about the excitation of atoms and molecules by electron impact.

In this review, we discuss studies of the chemoionization and quenching of excited atoms that are accompanied by the emission of fast electrons. Particular attention is devoted to the least studied problem, namely, chemoionization with the participation of two excited atoms. Different methods of investigating processes with the emission of fast electrons are examined, including the new technique of plasma electron spectroscopy (PES), based on the registration of electron spectra emitted in the corresponding reactions in plasmas.

1. PRODUCTION OF FAST ELECTRONS AND METHODS OF INVESTIGATING THEM

As noted above, there is particular interest in processes in which collisions between slow heavy particles result in the emission of ions and electrons, i.e., the chemoionization (CI) processes

$$A^* + B^* \rightarrow A^+ + B + e + \{\varepsilon_P\}, \tag{1.1}$$

$$A^* + B^* \rightarrow AB^+ + e + \{\varepsilon_A\}, \tag{1.2}$$

or processes in which potential energy is transferred from the excited state to electrons (quenching, collisions of the second kind, superelastic collisions), i.e.,

$$A^* + e \rightarrow A + e + \{\varepsilon_l\}; \tag{1.3}$$

where A^* and B^* are different (or identical) excited atoms, A and B are ground-state atoms, A^+ and AB^+ are the atomic and molecular ions, respectively, and e is the energy-acquiring electron in channels (1.1)–(1.3) in which (1.1) is Penning ionization (PI) and (1.2) is associative ionization (AI).

1063-7869/93/030152-19$10.00

The energy of CI electrons depends on the ratio of excitation to ionization energies of the partners prior to collision. If the resultant excitation energy $E_{1A}+E_{1B}$ of atoms A^* and B^* in the entrance channel of the reaction is much greater than the ionization energy of the atom (E_{A^+}) or the molecule E_{AB^+}, then fast electrons are emitted in reactions (1.1) and (1.2) with energy $\varepsilon_{P,A} \approx E_{1A} + E_{1B} - E_{A^+}(E_{AB^+})$ for which $\varepsilon \gg kT_e$ where T_e is the temperature of the Maxwellian part of the plasma electron velocity distribution. This case includes, for example, CI with the participation of excited atoms of hydrogen, inert gases, oxygen, and so on. In asymmetric collisions, reactions (1.1) and (1.2) with the production of fast electrons can also occur with the participation of excited and ground-state atoms when the energy of the excited atom is significantly greater than the ionization energy of a partner. The distinguishing feature of CI processes is that ionization and the acquisition of kinetic energy by the particles (in the first instance by electrons) occurs at the expense of internal excitation energy.

There is now a considerable volume of experimental and theoretical information about the parameters of reactions (1.2)–(1.3) (see, for example, Refs. 1–5).

The principal channels in which the above processes affect the properties of low-temperature plasmas have also been identified.[6] It is clear from (1.1)–(1.3) that this is a manyfaceted phenomenon. Actually, these reactions lead directly to the loss of excited states and to the appearance of electrons and a variety of ions. They can therefore lead to a change in the charged-particle concentration, and can determine the ion composition of plasma and the type of ionization and recombination.

When the characteristics of these processes are examined, particular attention will be devoted to the group of inert gases in which these reactions always occur with the emission of fast electrons.

Since excited atoms participate in processes (1.1) and (1.2), and charged particles with different masses and energies (electrons and molecular or atomic ions) are emitted in these reactions, the characteristics of the ionization process may be investigated (a) by studying changes in the concentration of excited atoms, (b) by using mass-spectroscopic techniques, and (c) by employing electron spectroscopy.

Until recently, reactions (1.1) and (1.2) in inert gases were usually investigated either in afterglow plasmas or in overtaking beams.

The two-body interaction constants for excited atoms in plasmas can be determined by calculating and measuring the concentration of the relevant atoms as a function of time. Such studies have been relatively infrequent because of the competition due to other, more effective, channels for the decay of the excited states under investigation, especially radiative channels.

Mass spectroscopy of afterglow plasmas has been used to examine the relative yields of molecular and atomic ions in collisions between excited atoms (He^*-He^*, Ne^*-Ne^*, and Ar^*-Ar^*). However, according to the review paper in Ref. 1, there is a discrepancy by an order of magnitude between the different reported data for the most commonly examined case, i.e., He^*-He^*. The difficulties encountered in mass-spectrometric diagnostics of reactions (1.1) and (1.2) in plasmas are associated with the following factors. First, the collision chamber (plasma-filled volume) and the ion analyzer are spatially separate, which means that the ion composition of the charged-particle flux may change on its way to the analyzer. Second, atomic and molecular ions in plasmas may originate not only in reactions (1.1) and (1.2), but also in competing processes such as, for example, Hornbeck-Molnar processes or processes involving the conversion of atomic ions into molecular ions in three-body collisions. Third, there are specific difficulties with the calibration of the sensitivity of the analyzer to different types of ion.

The overtaking-beam technique has been used to investigate the cross sections for reactions (1.1) and (1.2) in the energy range 0.01–10 eV in the case of He^*-He^*, Ne^*-Ne^*, and Ar^*-Ar^* (Ref. 1). The ion composition of the products of reactions (1.1) and (1.2) was also studied in Ref. 1. However, the results suffer from the absence of selection of different types of metastable atoms.

The above brief review shows that, in the few chemoionization experiments that have been performed, there was one reaction product that was not used, namely, fast electrons. In view of this, it is useful to compare methods (a)–(c) in relation to reactions (1.1)–(1.2) from the standpoint of the information that can be deduced from such data about the collision process.

The following collision characteristics are of interest: (1) the cross sections for reactions (1.1) and (1.2) as functions of the relative energy of the colliding particles, (2) the reaction constants as functions of the temperature of the colliding particles, (3) the energy spectrum of ions produced in these reactions, (4) the energy spectrum of electrons from these reactions, (5) the electron angular distribution, (6) the energy state of the molecular ions, (7) the potential energy curves in entrance and exit channels, and (8) the width of the autoionization term of the quasimolecule A^*B^*.

Method (a) can be used to solve problems (2) or (1), depending on the particular modification used. Mass-spectrometric diagnostics will, at least in principle, yield characteristics (1)–(3) and, to some extent, (7), i.e., the well depth of the quasimolecule. However, it is only electron spectroscopy that will yield all the collision characteristics enumerated above. The maximum amount of information about reactions (1.1) and (1.2) is therefore obtained by investigating the energy spectra of emitted electrons.

It was noted earlier that reactions (1.1) and (1.2) can be investigated in the afterglow plasma or by using the beam technique. The afterglow plasma has definite advantages associated with the relatively high concentration of excited atoms (10^{10}–10^{12} cm^{-3}) including those in radiative states. Beam experiments enable us to perform experiments at fixed colliding-particle energies, but this gives rise to obvious difficulties with the production of two excited-particle beams of sufficient intensity (especially in the case of atoms in radiative states).

So far, reaction (1.3) has not been discussed in detail. It will be sufficient to note that studies of this reaction in afterglow plasmas that rely on the direct reaction product, i.e., fast electrons, enable us to find the reaction rate constant as a function of electron temperature and the cross section as a function of energy.

The foregoing discussion leads us to the conclusion that it would be desirable to investigate processes (1.2)-(1.3) by a new method that combines the advantages of studies of elementary processes in plasmas with those of electron spectroscopy, i.e., plasma electron spectroscopy.

To solve the problem just posed, we have to analyze the relation between the plasma electron-energy distribution and the elementary processes (1.1)-(1.3), and on this basis develop experimental methods for determining the basic characteristics of these processes.

We now turn to a systematic examination of the above questions and then consider the data obtained by studying processes (1.1)-(1.3) and the effect of these processes on the properties of plasmas.

2. PLASMA ELECTRON ENERGY DISTRIBUTION AND PLASMA ELECTRON SPECTROSCOPY

The PES method relies on the relation between the electron-energy distribution for current-free plasma (including, in particular, the afterglow plasma) and the characteristics of the different elementary processes.

The evolution of the electron distribution function in plasma is discussed in detail in Refs. 4 and 6 for different conditions, taking (1.1)-(1.3) into account. In this review, however, we confine our attention to published results in so far as they are directly relevant to the principles of the PES method. With this in view, we consider the form of the distribution function in afterglow plasma when the mean free path λ is much smaller than the radius R of the tube. The transport equation for the isotropic part of the distribution function $f_0(\varepsilon,r)$ in cylindrical geometry with $\varepsilon \gg kT_e$ can be written in the form

$$\frac{1}{r}\frac{\partial}{\partial r}\left(rvD_r\frac{\partial f_0}{\partial r}\right)+\frac{\partial}{\partial \varepsilon}\left[v\left(D_\varepsilon\frac{\partial f_0}{\partial \varepsilon}+V_\varepsilon f_0\right)\right]$$
$$=\beta_m N_m^2 R_m(W)v+\beta_e N_m N_e R_e(W)v=0. \qquad (2.1)$$

In this expression, r is the radial coordinate, $\varepsilon(mv^2)/2+e\varphi(r)$ is the total energy, $\varphi(r)$ is the radial potential, and $D_\varepsilon=W(\delta\nu_a T_a+\nu_e T_e$ and $V_\varepsilon=W(\delta\nu_a+\nu_e)$ are the diffusion and dynamic friction coefficients in energy space, ν_e and ν_a are the electron-electron and elastic electron-atom collision frequencies, $\delta=2m/M$ is the energy transfer coefficient, T_e and T_a are the electron and atom temperatures, respectively, $D_r=v\lambda/3$ is the electron free-diffusion coefficient, β_m, R_m and β_e, R_e are the rate constants and energy spectra for (1.1)-(1.3), respectively, and N_e, N_m are the concentrations of electrons and atoms in excited states. The functions R_m, R_e are normalized so that

$$\int_0^\infty R_{m,e}(W)W^{1/2}dW=1. \qquad (2.2)$$

The boundary condition for $f_0(\varepsilon,r)$ on the tube wall when $\varepsilon>e\varphi(R)$ is

$$\frac{\varepsilon-e\varphi(R)}{4\varepsilon}f_0(\varepsilon,R)=-\frac{1}{3}\lambda\left.\frac{\partial f_0}{\partial r}\right|_{r=R}. \qquad (2.3)$$

We note that electron excitation processes are neglected in (2.1). The form of the distribution function when the corresponding term is taken into account is analyzeed in the Ref. 7 where the conditions for this term to be negligible are obtained.

For the sake of simplicity, it is assumed in (2.1) that all the atoms participating in reactions (1.1)-(1.3) are in the same excited state with concentration N_m. When several excited states have to be taken into account, the corresponding terms in (2.1) must be written down additively in the form of a sum. In weakly-ionized gas-discharge and current-free plasmas, the role of excited states is taken up by metastable levels or a set of low-lying long-lived resonant and metastable states whose population is much greater than the populations other excited states and is usually comparable with or greater than the charged-particle concentration. In photoplasmas, the relevant level is a resonant state pumped by an external source of radiation, and so on.

In the PES method, the experimental conditions are chosen so that the energy of the fast electrons emitted in reactions involving excited atoms does not change appreciably as a result of electron-electron and electron-atom collisions within the volume of the chamber, and the electrons diffuse freely toward the walls with a characteristic time $\tau_{df}=\lambda^2/D_r(\lambda=R/2.4$ is the diffusion length). Accordingly, in this case, the relaxation parameter is $k=(\nu_e+\delta\nu_a)\tau_{df}<1$.

To obtain the relationship between the characteristics of reactions (1.1)-(1.2) and the measured parameters, we must integrate the transport equation (2.1) over the spectra of the above reactions. Since the energy flux outside the integration range is zero, the second term in (2.1) disappears and the subsequent integration with respect to r, subject to the boundary condition

$$\left.\frac{\partial S_e}{\partial r}\right|_{r=0}=0, \quad S_e(R)=0 \qquad (2.4)$$

for the number S_e of fast electrons, gives

$$S_e^j(r)=\frac{\beta_j}{D_r(W_j)}\int_r^R\frac{dr'}{r'}\int_0^{r'}N_m(r'')N_j(r'')r''dr'', \qquad (2.5)$$

where the subscripts $j=m$,e refer, respectively, to reactions (1.1), (1.2) and (1.3) and W_j is the electron appearance energy in these reactions (ε_P, ε_A, or ε_1). It is clear from (2.5) that, to determine the constants β_j, we have to use absolute measurements of the electron distribution function (e.g., on the tube axis) to find the fast-electron concentration $S_e^j(0)$, then measure the absolute radial dependence of the concentrations $N_m(r)$ and $N_e(r)$ of excited atoms and electrons, respectively, and, finally, calculate the free diffusion coefficient $D_r(W_j)$ for the fast electrons.

In particular, when we consider two-particle collisions, for which the radial distributions of N_m and N_j are Bessel functions with the root $\mu_1=2.4$, we find from (2.5) that

$$S_e^j(0)=0.78\beta_j N_m(0)N_j(0)\tau_{df}.$$

Thus, in the above PES method, the rate constants of the elementary processes are determined from a direct product of the corresponding reaction, i.e., fast electrons.

We note that the PES can be used to solve two groups of problems. The first consists of determinations of the rate constants of elementary processes, and has been examined above. It involves the measurement of the integrated electron spectrum, i.e., the fast electron concentration S_e^j, which does not demand high resolving power in the measurement of the distribution function. The second group involves obtaining detailed information about reactions (1.1), and (1.2), i.e., the efficiency of Penning and associative ionization, the shape of the potential energy curves in the entrance and exit reaction channels, and the energy state of the molecular ion produced in the process. This involves investigations of the structure of the electron spectrum $R_m(W)$, and integral data are not sufficient.

Experimental conditions for which $k \ll 4T_e/W_j \ll 1$ are preferable in studies of reaction spectra. It is shown in Ref. 8 that the distribution function then has a peak near W_j which reproduces the shape of the energy spectrum of the corresponding reaction. The broading of the spectrum by the radial electric field can then be usually neglected.[8]

When $4T_e/W_j \leqslant k \leqslant 1$, the broadening of the original spectrum by elastic electron-atom and electron-electron collisions becomes significant. The broadening can be obtained by taking the source in the form of the δ-function

$$R_j(W)=\delta(W-W_j)/W_j^{1/2}$$

and writing the first term in (2.1) in the form $-vf_0/\tau_{df}$. The solution of (2.1)

$$f_0(\varepsilon,r)=\frac{\beta_j N_m(r)N_j(r)\theta(W_j-\varepsilon)}{\varepsilon^{3/2}(\nu_e+\delta\nu_a)} \times\exp\left(-\int_\varepsilon^{W_j}\frac{d\varepsilon}{\varepsilon(\nu_e+\delta\nu_a)\tau_{df}}\right) \qquad (2.6)$$

is then found to correspond to the instrumental function for broadening due to electron-electron and electron-atom collisions $A(\varepsilon,r)=f_0(\varepsilon,r)$ in the sense that the resultant distribution function is a convolution of the two energy spectra $R_j(W)$ and $A\Phi$, i.e.,

$$f(\varepsilon,r)=\int_0^\infty R_j(\varepsilon-x)A(x,r)dx. \qquad (2.7)$$

In equation (2.6),

$$\theta(z)=1,\quad z\geqslant 0,$$
$$=0,\quad z<0.$$

Thus, in the general case, the spectrum R_j must be found from measurements of the distribution function by solving the integral equation. However, as noted above, and is clear from (2.6), it is not essential for the condition $k\ll 4T_e/W_j \ll 1$ to be satisfied in these experiments.

3. EXPERIMENTAL METHODS

It was shown in the last Section that the rate constants and electron spectra in reactions (1.1)–(1.3) must be investigated in afterglow plasma whose parameters satisfy the condition $k \ll 1$. To obtain quantitative characteristics for reactions (1.1)–(1.13), we must measure the fast part of the distribution function, the electron concentration and temperature, and the radial distribution of the excited-atom concentration.

We shall now consider the different available methods, paying particular attention to measurements of the distribution function.

3.1. Measurement of the electron energy distribution

The electron energy analyzer used to determine the distribution function must meet the condition $\lambda \gg d$ where λ is the electron mean free path and d is a typical linear dimension of the analyzer. The pressure of the gas under investigation in the plasma volume is of the order of 0.1–5 Torr if $k\ll 1$ and the concentration of excited atoms is high (about 10^{10}–10^{12} cm^{-3}), so that the maximum possible value of d is found to be $d\approx 0.1$ cm. This means that traditional electron analyzers cannot be used under our conditions as they can be, for example, in Penning electron spectroscopy. At the same time, it is clear that the analyzer can take the form of a single electric probe, used under pulsed conditions to measure the electron velocity distribution function. In view of this, in our studies of reactions (1.1)–(1.3), we used the probe method of measuring the distribution function in plasmas with periodically varying parameters, based on probe current switching.[9]

We know[10] that the basic apparatus for Penning electron spectroscopy consists of four main parts, namely, a source of excited particles, a chamber in which collisions between excited particles take place, an electron-energy analyzer, and a recording system. In the PES method, the first and second parts are combined (the plasma volume performs this function) and, as already noted, the analyzer is an electric probe, which leads to a significant simplification of the opparatus.

The probe method of studying the distribution function is based on the relationship between this function and the second derivative of the electron current to the probe, given by the Druyvesteyn relation[11]

$$f(\varepsilon)\big|_{\varepsilon=eV}=(m^2/2\pi e^3S)d^2i_e/dV^2, \qquad (3.1)$$

where S is the probe area, V is the probe potential relative to the plasma potential, and i_e is the electron current to the probe.

In practice, the methods used to determine the distribution function differ mostly by the procedure used to obtain d^2i_e/dV^2. In our experiments, the second derivative of the probe current was determined by the modulation

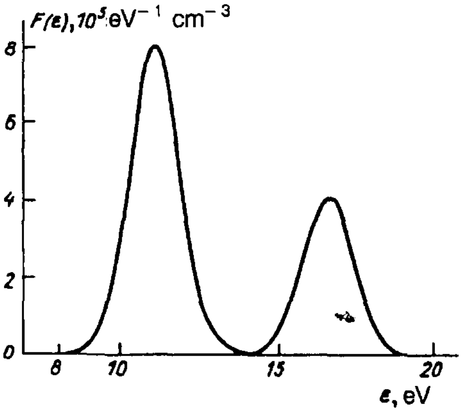

FIG. 1. Electron energy distribution in afterglow plasma in neon.

method[12] in which a small-amplitude alternating voltage (differentiating signal) is injected into the probe circuit and a harmonic of the probe current is recorded. The differentiating signal ΔV used in our studies was taken in the form

$$\Delta V_1 = 2V_1 \cos \omega_1 t, \tag{3.2}$$

$$\Delta V_2 = \sqrt{2} V_1 (1 + \sin \Omega t) \sin \omega_2 t. \tag{3.3}$$

It was shown in Ref. 13 that the amplitudes of the probe-current harmonics $I_{2\omega_1}$ at frequency $2\omega_1$ in the first case and I_Ω in the second case are related to the second derivative of the probe current with respect to the probe potential, i.e., $i''(V) d^2\pi / dV^0$ by the following expression:

$$I_{2\omega_1,\Omega} = V_1^2 \int_0^\infty i''(V') A_{1,2}(V,V') \mathrm{d}V' \equiv V_1^2 (i'' * A_{1,2}), \tag{3.4}$$

where A_1, A_2 are normalizing instrumental functions of the system used to measure the distribution function.

The probe method is described in greater detail in Ref. 4. The current sensitivity in the probe circuit at frequency $2\omega_1$ (for the differentiating signal ΔE_1) was 5×10^{-11} A. The minimum fast-electron concentration that could be recorded with probe radius of 4.5×10^{-3} cm, probe length 2 cm, and $2V_1 = 0.15$ V was 10^5 cm^{-3}. The total uncertainty in the measured distribution function in absolute measure did not exceed 25%.

Figure 1 shows the typical form of the fast part of the distribution function obtained experimentally in afterglow plasma.[14] The measurements were performed in neon at a pressure of 0.9 torr, current per pulse of 0.8 A, and delay after pulse end of 120 μs. It is clear from the figure that, in the energy range 8–20 eV, the distribution function has a complicated nonmonotonic shape. It can be explained by the appearance of fast electrons from reactions (1.1)–(1.3). Thus, the peak at 16.6 eV is due to collisions of the second kind between slow electrons and excited neon atoms in the $2p^5 3s$ state. The peak at 11 eV is due to interactions between excited neon atoms in the same states.

3.2. Determination of the temperature and concentration of electrons and the concentration of atoms

We determined the electron temperature from the measured $i''(V)$ curve, using the formula

$$T_e = 11600 \Delta V / \Delta \ln i''(V), \tag{3.5}$$

where T_e is the electron temperature in K and $\Delta \ln i''(V)$ is the change in the logarithm of the second derivative of the probe current within the potential interval ΔV (in V). Most of the electrons in afterglow plasmas have low energies, so that, provided their concentration is not too low, a Maxwellian distribution is established because of the strong electron-electron interaction, which in turn ensures that (3.5) is satisfied. The fact that T_e was determined correctly was confirmed by the fact that $\ln i''(V)$ was a linear function over a segment of sufficient length $(3kT_e - 4kT_e)$. The systematic uncertainty in the measured T_e did not exceed 10%.

The electron concentration N_e in decaying plasma was difficult to measure because of the specific properties of the afterglow, including low electron temperature, uncertainties in the measured plasma potential V_p, and distortions of the probe current near V_p.

Reliable values of N_e cannot obtained from the measured probe current at $V = V_p$ or by integrating the area under the $f(\varepsilon)$ curve. The concentration N_e is therefore best determined from the plasma conductivity either by the second-pulse method[15] in which an additional pulse is applied to the electrodes and the conductivity is measured during this pulse, or the conductivity (and therefore the plasma concentration) is measured during the active pulse and $N_e(t)$ is calculated afterward. The uncertainty in N_e is then about 30%.

Several methods are available for measuring the concentration of excited atoms in plasmas.[16] The intensity of lines emitted by afterglow plasma is low, so that the double-tube version of the absorption method is the most widely used and yields the concentration of atoms in low-lying energy states. The uncertainty in the measured excited-atom concentration obtained in this way is of the order of 20%.

After this brief survey of experimental methods, it is useful to compare once again traditional Penning electron spectroscopy with PES. Since information about the elementary processes is obtained in both PES and in Penning electron spectroscopy by analyzing the electron spectra of the corresponding reactions, the two methods are similar in scope. However, there are also significant differences because PES is used in plasmas whereas Penning spectroscopy relies on the interaction between atomic beams. In view of this, plasma electron spectroscopy has obvious advantages for the investigation of ionization processes with the participation of two excited atoms, especially if these atoms are in radiative rather than metastable states. It is precisely for this reason that, literally up to very recently, the electron spectra of chemoionization processes involving two excited atoms could only be obtained by PES. The fact that optical methods of measuring the concentration of excited atoms can now be used in PES, means that, in contrast to Penning spectroscopy, high-precision absolute measurements are possible. The energy resolving power of Penning spectroscopy is at present better by a factor of 5–10 as compared with PES. We also note that Penning spectroscopy enables us to obtain the reaction cross sections as functions of the energy of the colliding particles, and also the angular distribution of the emitted electrons. The PES method can be used to determine the rate constant for different atomic temperatures of the colliding particles. It is well known that the rate constant is an average evaluated over the velocities of the interacting particles and the electron scattering angles. It carries information about the cross section for the process.

Penning electron spectroscopy has by now produced an extensive literature on ionizing processes involving excited particles. The results, and also a detailed description of the method itself, can be found in review articles and monographs, for example, those given in Refs. 3 and 10. We shall confine our discussion to the results obtained by Penning spectroscopy and also by mass-spectrometric and optical methods, in so far as they are directly relevant to the theme of our review here.

4. STUDIES OF THE INTERACTION BETWEEN EXCITED INERT-GAS ATOMS

4.1. Determination of chemoionization rate constants

We have investigated ionization processes involving inert-gas atoms in identical or different excited states. It is clear from (2.5) that, depending on the concentrations $N_m^{(i)}, N_m^{(k)}$ of the different excited atoms and the magnitude of the corresponding constants $\beta_m^{(i,k)}$, the distribution function will exhibit features associated with one or several reactions. The selection of two-body reactions involving excited atoms in different states is performed in PES either directly on the basis of their electron spectrum (if they are separated) or from the variation in the intensity of the electron spectrum with the relative concentration of excited states.

The measurements were performed under the following conditions. A periodic pulsed discharge in helium, neon, argon, krypton, or xenon was initiated in a cylindrical glass tube with a diameter of 30–40 mm and cold electrodes. The duration of the active phase was 10–90 μs, the pulse repetition frequency was 0.5–5 kHz, and the current was 0.01–2 A. The gas pressure was varied in the range 0.1–2 torr. Fixed and mobile probes with diameters of 0.35–0.24 mm and lengths of 10–30 mm were inserted into the tube.

4.1.1. Helium. Six reactions involving the metastable atoms He(2^1S) and He(2^3S) and the metastable molecule $He_2(2^3\Sigma)$ can take place in helium afterglow. The concentration of the $He_2(2^3\Sigma)$ molecules that participate in the afterglow, mostly as a result of conversion and recombination reactions, becomes considerable at pressures above a few torr, and processes involving their participation were not investigated. Figure 2 shows[17] typical data on the distribution function in helium (pressure 0.2 torr, current per pulse 0.2 A, delay after the end of the pulse 50 μs, and peak-to-peak amplitude of the differentiating signal *1* V). The peak at 14.4 eV is due to the He(2^3S)-He(2^3S) reaction, the peak at 15.4 eV is due to the He(2^3S)-He(2^1S) reaction, and the peak at 16.2 eV is due to the He(2^1S)-He(2^1S) reaction. It is clear from the figure that the second and third peaks on curve *1*, which is broadened by the instrumental function, cannot be resolved. This complicates the determination of the rate constant for the reaction with the participation of the metastable 2^1S-2^1S atoms. To find the true distribution function from the experimental data, the latter were analyzed by the Tikhonov regularization procedure[18] since equation (3.4) is a Fredholm equation of the first kind whose kernel is the instrumental function A_2. The result of this procedure[17] is also shown in Fig. 2 (curve *2*). Since the electron spectra of different reactions overlap, we use measurements of the distribution function for different ratios of the concentration of atoms in 2^3S and 2^1S states to separate them (dashed curve). This allows us to observe either the peak at 14.4 eV alone, or the two peaks at 14.4 and 15.4 eV, or all three peaks together. The electron spectra obtained in this way were used to determine the reaction rate constants. To reduce systematic errors in the constants $\beta_m(2^3S,2^1S)$ and $\beta_m(2^1S,2^1S)$, we took advantage of the fact that the reaction rate constant $\beta_m(2^3S,2^3S)$ is well known and its value averaged over a large number of measurements[19,20] is $(0.9\pm0.1)\times10^{-9}$ cm^{-3} s^{-1}. In the case of curve *1* in Fig. 2, the concentration of the helium atoms in 2^3S and 2^1S states at the center of the tube was 4.1×10^{11} and 8.0×10^{10} cm^{-3}, respectively.

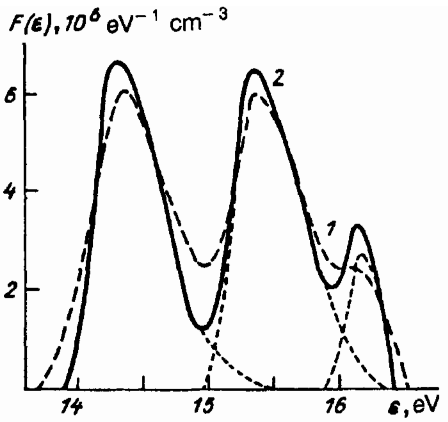

FIG. 2. Electron energy distribution in helium: *1*—experimental, *2*—calculated by the regularization method.

Table I lists the values of β_m calculated from (2.5) using the experimental data, and also the capture rate constants k_m for collisions between these atoms. These constants were calculated from the formula[21]

$$k_m=\alpha\gamma 2^{-1/6}\pi^{1/2}\cdot 6\Gamma(5/3)C_6^{1/3}(kT_a)^{1/6}\mu^{-1/2}, \quad (4.1)$$

where $\alpha=1$ for atoms of different type and $\alpha=1/2$ for atoms of the same type, γ is a factor representing the conservation of spin (4/9 for 2^3S-2^3S and 1 for the other two pairs), Γ is the gamma-function, C_6 is the van der Waals interaction constant, μ is the reduced mass of the colliding

TABLE I. Reaction constants and cross section for the ionization and capture processes with the participation of two excited inert-gas atoms.

Reaction	β_m, 10^{-9} $cm^3 s^{-1}$	k_m, 10^{-9} $cm^3 s^{-1}$	$\bar{\sigma}_\beta$, 10^{-15} cm^2	$\bar{\sigma}_k$, 10^{-15} cm^2
1. $He(2^3S)$—$He(2^3S)$	0,9±0,1 [19]	0,92	5,0±0,5	5,1
2. $He(2^3S)$—$He(2^1S)$	4,0±0,5	4,92	22,5±3,0	27,6
3. $He(2^1S)$—$He(2^1S)$	4,1±0,9	3,36	23,0±5,0	18,9
4. $Ne(^3P_2)$—$Ne(^3P_2)$	0,38±0,04	0,86	4,8±0,5	10,8
5. $Ne(^3P_2)$—$Ne(^3P_1)$	1,3±0,4	1,59	16±5	20,0
6. $Ar(^3P_2)$—$Ar(^3P_2)$	1,2±0,2	0,81	22±4	14,4
7. $Kr(^3P_2)$—$Kr(^3P_2)$	1,1±0,2	0,52	29±5	13,5
8. $Xe(^3P_2)$—$Xe(^3P_2)$	0,19±0,03	0,48	6,2±0,9	15,4

atoms, and T_a is the temperature of the atoms, which, in our case, was 300 K. The values of C_6 were taken from Ref. 22.

Table I lists the values of the constants with an indication of the random measurement error and without the separation of the Penning and associative ionization channels. These data characterize the rate at which fast electrons are produced in these reactions and are equal to the rate constants for the disappearance of excited atoms in processes with the participation of atoms of different type. They should be multiplied by two when we consider the rate of disappearance of excited atoms in symmetric collisions. Table I also lists values of the effective cross section, defined as the ratio of the corresponding rate constant for the process to the mean relative velocity of the atoms

$$\bar{\sigma}_\beta=\beta_m/(8kT_a/\pi\mu)^{1/2}. \qquad (4.2)$$

It is clear from Table I that the rate constants measured in helium are close to the calculated capture rate constants, indicating a high efficiency of autoionization of the quasimolecules produced in collisions between excited atoms.

It is important to note that, under certain specific conditions, reactions involving metastable atoms can contribute to the evolution of the distribution function in plasmas other than the current-free plasma. For example, peaks were observed on the distribution function obtained in a helium discharge of a particular configuration.[23] They were due to reactions (1.1)–(1.3), and the corresponding rate constants were calculated.

4.1.2. Neon and argon. The above method was also used to determine the reaction rate constants for excited atoms in the afterglow of neon in $2p^53SP_2,^3P_1,^3P_0$ states and argon in $3p^54s^3P_2$ states (Refs. 14 and 24). The $^3P_2$ and $^3P_0$ levels are metastable whereas $^3P_1$ are radiative. As far as we know, there are no previous direct data on these constants. A weighted average based on all four levels of the $2P^53S$ configurations of neon was obtained in Ref. 25 for the rate constants, using an analysis of the ionization balance in the discharge. The mean cross section for the process deduced from this constant was 10^{-14} cm^2. The same approach was adopted in Ref. 26 to determine the cross section for the two-body interaction between excited atoms, and the result was 4×10^{-15} cm^2.

In principle, there are ten possible two-body reactions with the participation of atoms in $^3P_2,^3P_1,^3P_0,^1P_1$ states. Because of the small level separation (a few hundredths of eV), the spectra due to these reactions could not be separated and measurements had to be performed for different ratios of excited-atom concentrations, followed by a solution of the corresponding set of equations. It was found that it was impossible to determine all ten constants from the resulting set of equations because some of the reactions give a negligible contribution to the total fast-electron concentration (much smaller than the random measurement uncertainty), so that the set of equations was not stable. A preliminary estimate of the expected rate constants for the corresponding reactions had to be made using (4.1). The constants C_6 for neon and argon atoms (and, later, for krypton and xenon) were calculated from the Slater–Kirkwood formula[21] in which the factor γ was taken equal to unity because it was not known whether the spin conservation rule was satisfied in the decay of the quasimolecule.[2]

The observed fast part of the distribution function for the neon afterglow plasma is shown in Fig. 1. The peak at 11 eV was used to find the concentration of fast electrons $S_e^{1,k}$ and the rate constants $\beta_m^{i,k}$. The concentration of atoms in the $^1P_1$ state under the chosen conditions of measurement was usually lower by two orders of magnitude than the concentration of $^3P_2$ atoms. The experimental data (obtained under more than ten different conditions) were used to set up a set of equations which was solved by the method of least squares. The three constants $\beta_m^{(2,2)}$, $\beta_m^{(2,1)}$, and $\beta_m^{(2,0)}$ were taken into account in the calculation. Here and henceforth the inert-gas states $^3P_2$, $^3P_1$ and $^3P_0$ will be indicated by subscripts 2, 1 and 0, respectively. The values of the first two constants obtained in this way are listed in Table I. Only an estimate is possible for the third constant: $\beta_m^{(2,0)}<5\times10^{-10}$ cm^3 s^{-1}. If the constants ignored in the calculation are assumed equal to the capture constants, this changes the magnitude of $\beta_m^{(2,2)}$ by not more than 2% and the value of $\beta_m^{(2,1)}$ by not more than 10%, which confirms the validity of these calculations. Since the concentration of $3P^54S^3P_2$ atoms in the argon afterglow accounts for 70 and 95% of the concentration of all the excited atoms in this configuration, only the constant $\beta_m^{(2,2)}$ was determined (see Table I).

The values obtained by the same method in Refs. 27 and 28 were as follows: $\beta_m^{(2,2)}=(0.37\pm0.1)\times10^{-9}$ cm^3 s^{-1} for neon and $\beta_m^{(2,2)}=(1.3\pm0.4)\times10^{-9}$ cm^3 s^{-1} for argon, which is in good agreement with the data in Table I.

4.1.3. Krypton and xenon. The requirement that free diffusion of fast electrons predominated over energy relaxation ensured that correct measurements of β_m in krypton and xenon in a 3.5-cm diameter tube were obtained at pressures $p\leqslant0.5$ torr and discharge currents $i\leqslant40$ mA. The resultant population of $3P_1$, $^3P_0$, and $^1P_1$ levels did not

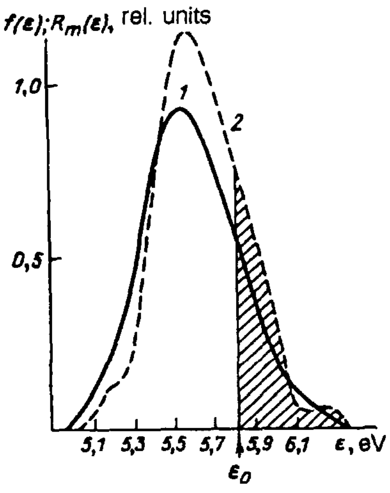

FIG. 3. Experimental electron velocity distribution $f(\varepsilon)$ in krypton (*1*) and the reconstructed electron spectrum $R_m(\varepsilon)$ (*2*). Pressure 0.5 torr, current per pulse 10 mA, delay 200 μs.

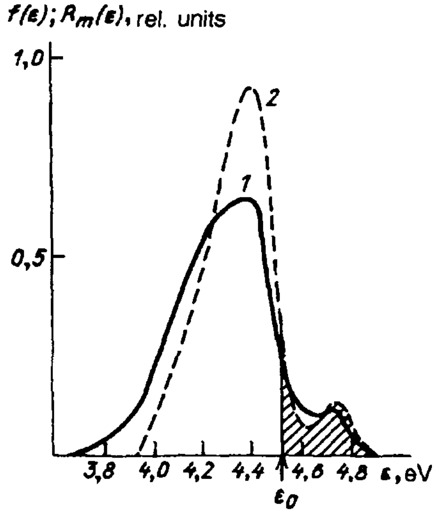

FIG. 4. Experimental electron velocity distribution in xenon (*1*) and the reconstructed electron spectrum (*2*). Pressure 0.2 torr, current per pulse 40 mA, delay 350 μs.

then exceed 3% of the $^3P_2$ population (Refs. 29–31). The rate constants found in this way are listed in Table I. The measured value of $\beta_m^{(2,2)}$ obtained in Ref. 32 for krypton was $(1.8\pm0.4)\times10^{-9}$ cm^{-3} s^{-1} (the same method of measurement was employed). The same authors[33] reported $\beta_m^{(2,2)}=(7.6\pm1.0)\times10^{-10}$ cm^3 s^{-1} for xenon. In the measurements of the metastable-atoms concentration in xenon reported in refs. 29–31, the corresponding transition probability was assumed to be $A_{ki}=2\times10^6$ s^{-1} (Ref. 34). However, if the more recent result[35] $A_{ki}=0.72\times10^6$ s^{-1} is employed, the corresponding rate constant becomes $\beta_m^{(2,2)}=1.9\times10^{-10}$ cm^3 s^{-1} which agrees with Table I.

4.2. Electron spectra of chemoionization processes

As already noted, the most detailed information about reactions (1.1) and (1.2) is obtained by investigating the electron spectra emitted in these reactions. The distribution functions recorded with the smallest possible differentiating-signal amplitude (1 V peak-to-peak in helium and 0.3–0.4 V in krypton and xenon) were used to solve the inverse problem and hence to find the electron spectra $R_m(\varepsilon)$. The necessary calculations were performed by E. A. Kral'kina at the Computational Center of the Moscow State University, using the functions A, $A_{1,2}$ or their convolution as the kernels of the integral equation. The absolute calibration of the energy scale was made using the peak on the distribution function due to the reaction (1.3). This method of calibration ensured a precision of 0.1 eV in helium, 0.02 eV in krypton, and 0.04 eV in xenon. The measured distribution functions and the reconstructed electron spectra emitted in the chemoionization processes involving two metastable $3P_2$ atoms of krypton and xenon are shown in Figs. 3 and 4. As far as we know, there have been no experimental studies of the electron spectra of chemoionization processes involving two excited atoms prior to the publication of Ref. 4. A complete calculation of this spectrum for the He(2^3S)-He(2^3S) ionization reaction was reported in the theoretical paper in Ref. 36, but it did not take into account the overlap of the spectra from the Penning and associative ionization reactions, which is of fundamental importance to the practical application of electron spectroscopy. This question is examined in some detail in Ref. 37. The point is that calculations of the overlap of these spectra encounter a difficulty associated with the inclusion of quasistationary states produced in electronic transitions in the effective potential in the exit channel of the reaction. Depending on the experimental conditions, there are then two possible formulations of the problem,[38] namely, the 'classical formulation', in which the centrifugal barrier is assumed to be impenetrable, and the 'quantum-mechanical formulation', in which this barrier is assumed to be completely transparent. It was shown in Ref. 37 that the maximum width $\Delta\varepsilon$ (eV) of the overlap region between the associative and Penning ionization is given by

$$\Delta\varepsilon=0.9(R_{ie}D_i^{1/6}/R_{fe}D_f^{1/4})^4E_0^{4/3}, \tag{4.3}$$

where R_{ie},R_{fe} are the equilibrium distances between the potential energy curves in the initial and final states, D_i,D_f are their depths in eV, and E_0 is the energy of the colliding particles (in eV).

Table II, which is taken from Ref. 37, lists the corresponding data for symmetric collisions between excited inert-gas atoms. In several cases, we use the similarity between metastableinert-gas atoms and alkali-metal atoms. The low value of $\Delta\varepsilon$ as compared with the total width of the spectrum (of the order 1 eV) suggests that the fraction Q of the yield of molecular ions in the total ion yield is very similar in classical and quantum-mechanical approaches. It is then possible to neglect the influence of quasistationary states (whose appearance is related to the centrifugal barrier) on the efficiency of production of molecular ions.

The velocity distribution of the colliding particles can give rise to an additional overlap of associative and Pen-

TABLE II. Term parameters of initial (R_{ie},D_i) and final (R_{fe},D_f) states and the width of the overlap between the associative and Penning ionization $\Delta\varepsilon$ at $E_0=0.026$ eV.

Colliding atoms	R_{ie}, a_0	D_i, eV	R_{fe}, a_0	D_f, eV	$\Delta\varepsilon$, eV
$He(2^3S)$—$He(2^3S)$	6,5 [36]	0,6 [36]	2 [36]	2,5 [36]	0,22
$Ne(^3P_2)$—$Ne(^3P_2)$	5,9 [21]	0,75 [21]	3,2 [40]	1,17 [40]	0,06
$Ar(^3P_2)$—$Ar(^3P_2)$	7,4 [39]	0,52 [39]	4,8 [21]	1,23 [21]	0,02
$Kr(^3P_2)$—$Kr(^3P_2)$	7,8 [39]	0,49 [39]	5,4 [21]	1,15 [21]	0,02
$Xe(^3P_2)$—$Xe(^3P_2)$	8,3 [39]	0,45 [39]	6,3 [21]	1 [21]	0,01

ning ionization spectra. The analysis reported in Ref. 37 for the electron spectrum from the $He(2^3S)$-$He(2^3S)$ reaction averaged over the Maxwellian distribution of the atoms with $T_a=300$ K has shown that the magnitude of this overlap, corrected for the additional broadening of the order of kT_a, is in good agreement with estimates based on (4.3).

The spectrum calculated in this way was then used to show that $Q=10\%$ in the quantum mechanical calculation and $Q=14\%$ in the classical approxiamtion. Consequently, whenever an experimental electron spectrum is available, a reliable estimate of Q can be obtained by dividing the spectrum into two parts at $\varepsilon_0=\varepsilon_\infty+kT_a$ where $\varepsilon_\infty = 2E_{1A} - E_{A^+}$. Electrons produced in associative ionization then correspond to energies $\varepsilon>\varepsilon_0$ whereas those from Penning ionization corresponds to $\varepsilon\leqslant\varepsilon_0$. The molecular-ion yield obtained in this way is listed in Table III.

We note that this apparently natural subdivision of the spectrum is in conflict with the results reported in Ref. 6 where Q is calculated for the $He(2^3S)$-$He(2^3S)$ reaction. According to Ref. 36, $Q\gg80\%$ in the thermal energy region, which should be an indication of the considerable overlap of the Penning and associative ionization spectra and the fact that the experimental total electron spectrum cannot be used to determine Q. However, checks have shown that[37] the calculations of Q reported in Ref. 36 are subject to an error. The yield of molecular ions from the $He(2^3S)$-$He(2^3S)$ reaction listed in Table III and reported in Ref. 37 is in agreement with the data from Ref. 1, which were obtained by the mass-spectrometric method for overtaking beams ($Q=4.6\pm0.6\%$), and also with the calculations reported in Ref. 37. For the $He(2^3S)$-$He(2^1S)$, $Kr(^3P_2)$-(Kr^3P_2), and $Xe(^3P_2)$-$Xe(^3P_2)$ pairs, the molecular-ion yield of chemoionization reactions was determined for the first time in Ref. 4. Similar experiments were also performed in neon, but the sensitivity of the apparatus was inadequate so that only an estimate could be obtained: the molecular ion yield in the $Ne(^3P_2)$-$Ne(^3P_2)$ reaction was found to be $Q<25\%$.

A recent paper[41] has reported an electron-spectroscopic study of ionization in two-body collisions between metastable helium atoms in 2^3S and 2^1S states in beam experiments. The electron spectra of these reactions were obtained with a high energy resolution (36 and 70 meV). Carefully calculated ionization cross sections, electron spectra, and relative molecular ion yields were compared with experimental data. The values of Q for helium listed in Table III agree to within experimental uncertainty with the results reported in Ref. 31. A low measured molecular-ion yield in neon and carbon ($Q=7\%$ and 5%) was reported in Ref. 42. These measurements were made by a mass-spectrometric method in the afterglow of a pulsed high-frequency discharge.

The combined data obtained by PES and confirmed by other experiments lead to the conclusion that ionization in collisions between two excited inert-gas atoms produces mostly atomic ions (molecular ion yield $Q<25\%$). For these particular reactions, this appears to be due to the difference between the equilibrium nuclear separations in the initial and final states.

An interesting feature of the spectrum obtained for krypton and xenon (Figs. 3 and 4) is the secondary peak which corresponds to the classical turning point on the potential curve of the quasimolecule.

The fact that the widths of the electron spectra due to associative ionization are significantly smaller than the dis-

TABLE III. Parameters of the ionization reaction with the participation of excited inert-gas atoms.

Colliding atoms	ε_∞, eV	Q, %	Associative ionization spectrum width, eV	Energy of collisional excitation of molecular ion, eV	Measured value of D_i, eV
$He(2^3S)$—$He(2^3S)$	15,05	7 ± 4	≈ 0,5	> 2	0,9 ± 0,2
$He(2^3S)$—$He(2^1S)$	15,85	16 ± 6	≈ 0,5	> 2	0,6 ± 0,2
$Kr(^3P_2)$—$Kr(^3P_2)$	5,82	13 ± 6	0,5 ± 0,1	> 0,6	0,6 ± 0,1
$Xe(^3P_2)$—$Xe(^3P_2)$	4,49	12 ± 4	0,4 ± 0,1	> 0,6	0,4 ± 0,1

sociation energies D_f of the corresponding molecular ions (see Tables II and III) shows that, in slow collisions of excited helium, krypton, and xenon atoms, the resulting molecular ions are in highly-excited vibrational states. This conclusion is also valid for other pairs of inert-gas atoms[37] because it relies essentially on these substantial difference between the equilibrium separations in the initial and final state (this was used above to explain the low value of Q).

If we suppose that the equilibrium separation between the potential energy curves of quasimolecules corresponds to the flat portions of the corresponding potential energy curves of molecular ions, then the electron spectra can be used to deduce the dissociation energy D_i of the quasimolecules. This energy is determined by the energy width of the electron spectrum due to Penning ionization at 44% of the maximum peak height.[10] Its values are listed in Table III. There is a clear agreement between values of D_i obtained in this way and the data in Table II.

We know[43] that there are two possible states, $^2P_{1/2}$ and $^2P_{3/2}$, that correspond to the inert-gas ion configuration s^2p^5, where $^2P_{3/2}$ is lower than $^2P_{1/2}$ by 0.67 eV in krypton and 1.19 eV in xenon. The energies of the electrons produced in reactions (1.1) and (1.2) should differ by the same amount in the corresponding states. The presence of such a large gap as compared with the half-width of the instrumental function, which represents collisions and the finite amplitude of the differentiating signal, can be used, at least in principle, to separate these groups of electrons. Studies of the spectra $R_m(\varepsilon)$ have shown that atomic ions in the $^2P_{1/2}$ state and the corresponding molecular ions account for not more than 8% of the total number of ions in krypton and not more 6% in xenon.

5. PENNING IONIZATION OF ATOMS AND MOLECULES BY METASTABLE HELIUM ATOMS

It is clear that the PES method used above to investigate the interaction between excited atoms is directly applicable to Penning ionization with a participation of excited and normal atoms and molecules. There is considerable interest, from both theoretical and practical points of view, in the ionization of heavy inert gases such as argon, krypton, and xenon, and also molecular gases (carbon and nitrogen oxides), by metastable helium atoms.

5.1. Ionization of heavy inert-gas atoms

Interactions between $He(2^3S_1, 2^1S_0)$ and argon, krypton, and xenon are discussed in an extensive literature, critically reviewed in Ref. 19. The averages over existing data, evaluated in Ref. 19, show that only the ionization constants representing the ionization of xenon and krypton atoms by helium in metastable triplet states have been found with reasonable precision (uncertainty of 10–15%). The average values of the other constants are subject to uncertainties of 50–80%. The ratio β_{m1}/β_{m3} of ionization rate constants determined in this way for the metastable atoms $He(2^1S)$ and $He(2^3S)$ interacting with argon, krypton, and xenon are subject to comparable uncertainties. It was therefore decided to measure the ratio β_{m1}/β_{m3} by the new PES method which is free from the disadvantages of beam methods (the excited-atom concentration is difficult to measure) and methods relying on measurements of the excited-atom concentration as a function of time or position (which suffer from competing processes resulting in the loss of metastable atoms).

TABLE IV. Relative production rate of the ions of heavy inert gases in the $R^+(^2P_{3/2})$ and $R^+(^2P_{1/2})$ states in the $He(2^{3,1}S)+R$ reaction.

Ratio of constants	Inert gas			Reference
	Ar	Kr	Xe	
$\beta^{(3/2)}_{m3}/\beta^{(1/2)}_{m3}$	1,92	1,90	2,24	[47]
	1,94	1,80	2,03	[48]
$\beta^{(3/2)}_{m1}/\beta^{(1/2)}_{m1}$	2,04	1,60	1,45	[47]
	2,00	1,80	1,34	[48]

These reactions can proceed along channels (1.1) and (1.2). Mass spectrometry and electron spectroscopy in beams have produced[19,44] the relative yield of molecular heteronuclear ions in the $He(2^{1,3}S)+R$ reaction, where R is the inert-gas atom. Accordingly, the relative contribution of associative ionization to the total cross section for processes (1.1) and (1.2) was found to be not more than 10-15%. Penning ionization is the dominant process in the $He(2^{1,3}S)+R$ reaction.

Analysis of the electron spectra emitted in Penning ionization has shown[45–48] that, similarly to the interaction between two excited inert-gas atoms (see Section 4.2), the reactions

$$\xrightarrow{\beta^{(3/2)}_{m3}} He+R^+(^2P_{3/2})+e, \qquad (5.1)$$

$$He(2^3S_1)+R \xrightarrow{\beta_{m3}}$$

$$\xrightarrow{\beta^{(1/2)}_{m3}} He+R^+(^2P_{1/2})+e, \qquad (5.2)$$

$$\xrightarrow{\beta^{(3/2)}_{m1}} He+R^+(^2P_{3/2})+e, \qquad (5.3)$$

$$He(2^1S_0)+R \xrightarrow{\beta_{m1}}$$

$$\xrightarrow{\beta^{(1/2)}_{m1}} He+R^+(^2P_{1/2})+e \qquad (5.4)$$

produce R^+ ions in the $^2P_{3/2}$ and $^2P_{1/2}$ states. The $^2P_{1/2}$ term then lies above the $^2P_{3/2}$ term. In argon, the difference amounts 0.18 eV. The corresponding data for krypton and xenon were reproduced earlier.

Previous determinations[10,47,48] showed that the energy spectrum produced in the $He(2^{1,3}S)+R$ reaction and the shift of its maximum relative to ε_∞ had low values ($\leqslant$0.1 eV). The angular distribution of the resulting electrons was investigated in the limited scattering-angle range $\vartheta=20$–90° (Refs. 47 and 48). In particular, the relative yield of $R^+(^2P_{3/2})$ and $R^+(^2P_{1/2})$ ions at $\vartheta=90°$ was as listed in Table IV.

Thus, existing information was used in the PES method to achieve more reliable measurements of the Pen-

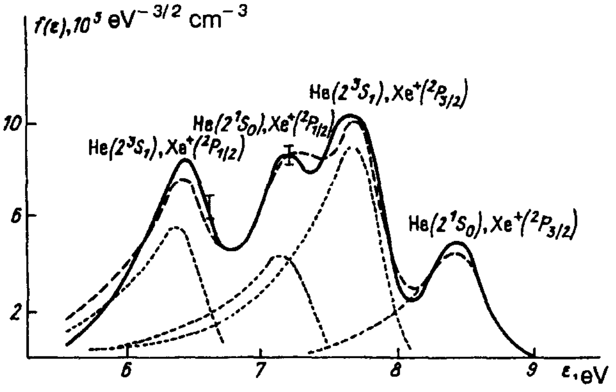

FIG. 5. Electron velocity distribution in the helium-xenon mixture. Pressure 0.8 torr of helium and 10^{-5} torr of xenon, current per pulse 42 mA, delay time 35 μs, $N_e = 2\times 10^{10}$ cm^{-3}, $N_m(2^3S) = 2\times 10^{11}$ cm^{-3}, $N_m(2^1S) = 5.2\times 10^{10}$ cm^{-3}, signal amplitude in (3.2), $V_1 = 0.15$ V.

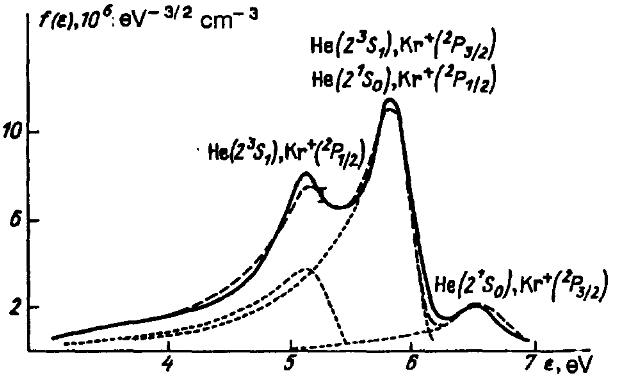

FIG. 6. Electron velocity distribution in the helium-krypton mixture. Pressure 0.35 torr of helium and 9×10^{-4} torr of krypton, current per pulse 85 mA, delay time 17 μs, $N_e = 3\times 10^{10}$ cm^{-3}, $N_m(2^3S) = 10^{11}$ cm^{-3}, $N_m(2^3S) = 1.3\times 10^{10}$ cm^{-3}, signal amplitude in (3.2) $V_1 = 0.1$ V.

ning ionization ratio β_{m1}/β_{m3} and to determine angle-averaged ratios of the constants describing ionization with the production of R^+ ions in the $^2P_{1/2}$ and $^2P_{3/2}$ states (such data are not available in the literature).

The measurements were performed[49] on the afterglow plasma of a pulsed discharge in a 1.9 cm diameter tube at helium pressure of 0.3–0.8 torr, heavy inert-gas impurity of 10^{-5}–10^{-8} torr, current per pulse 60–100 mA, discharge pulse length 10–20 μs, pulse repetition frequency 1 kHz, delay 60–100 μs, and electron density in the range 10^{10}–10^{11} cm^{-3}.

To ensure that the contribution of the second derivative of the ion current was correctly taken into account in the experimentally determined distribution function, the measurements of the second derivative of the probe current were under similar conditions in pure helium [which does not exhibit the peaks due to reactions (5.1)–(5.4)]. The corresponding curve was then used to determine the ion component in measurements on the He+R mixtures.

5.1.1. Helium-xenon mixture. Figure 5 shows a typical experimental distribution function for very comparable concentrations of triplet and singlet metastable helium atoms. In this case, the energy range 6–9 eV contains all four peaks due to reactions (5.1)–(5.4). It is clear that the observed peaks exhibit partial overlap. The curves due to the respective reactions were obtained from the experimental curves in the following way. In view of the foregoing discussion, and because the width of $R_m(\varepsilon)$ was small (this width, like the broadening due to the radial field, is much smaller than collision broadening within the volume and the finite width of the instrumental function of the aparatus), the function $R_m(\varepsilon)$ was represented by a delta function. Collision broadening and the finite width of the instrumental function of the aparatus were then taken into account, and a least-squares procedure was used to fit the function obtained in this way to the measured distribution function. Figure 5 shows the peaks (points) and the sum of peaks (dashes) obtained in this way. The result is clearly close to the experimental data (solid curve). All this gave the following ratios of production rates for the two states of Xe^+ ions in the $He(2^{3,1}S)+Xe$ reactions: $\beta^{(3/2)}_{m3}/\beta^{(1/2)}_{m3} = 2.4\pm 0.2, \beta^{(3/2)}_{m1}/\beta^{(1/2)}_{m1} = 1.3\pm 0.3$.

We emphasize that the PES value is an average over the scattering angles. It agrees to within the indicated uncertainty with the corresponding values listed in Table IV for $\beta = 90°$. Averaging of different measurements also yielded the result $\beta_{m1}/\beta_{m3} = 2.7\pm 0.5$. We note that the uncertainty in this result is substantially lower than the uncertainty in β_{m1}/β_{m3} obtained by averaging data reported by different workers. This ratio and the accurate result $\beta_{m3} = (15.3\pm 2.5)\times 10^{-11}$ cm^3 s^{-1} (Ref. 3) were used for $T_a = 300$ K to show that $\beta_{m1} = (4.1\pm 1.0)\times 10^{-10}$ cm^3 s^{-1}.

5.1.2. Helium-krypton mixture. The experimental distribution function obtained for the He+Kr plasma is shown in Fig. 6. Because of the smaller energy gap between the $^2P_{3/2}$ and $^2P_{1/2}$ states of the Kr^+ ion (it amounts to 0.67 eV), and in contrast to the He+Xe mixture, the peaks due to (5.1) and (5.4) are now seen to overlap completely.

The experimental curves were analyzed as follows in order to compare the yields of all four processes (5.1)–(5.4). As in the case of the xenon mixture, the partially overlapped peaks were first separated (cf. Fig. 6 which illustrates the procedure; the notation is the same as in Fig. 5). The ratio of the number of fast electrons in the second and third peaks and in the second and first peaks was then determined as a function of the ratio of the concentrations of metastable helium atoms in different states. This yielded $\beta^{(3/2)}_{m3}/\beta^{(1/2)}_{m3}, = 2.4\pm 0.4$ and $\beta^{(3/2)}_{m1}, /\beta^{(1/2)}_{m1} = 1.4\pm 0.4$.

The ratio β_{m1}/β_{m3} was found to be $\beta_{m1}/\beta_{m3} = 2.9\pm 0.5$ and the known result $\beta_{m3} = (11.3\pm 1.2)\times 10^{-11}$ cm^3 s^{-1} was used for $T_a = 300$K to show that $\beta_{m1} = (3.3\pm 0.7)\times 10^{-10}$ cm^3 s^{-1}.

5.1.3. Helium-argon mixture. For the argon ion, the energy gap between the $^2P_{3/2}$ and $^2P_{1/2}$ states is small (≈ 0.18 eV), so that PES does not allow us to separate the distribution-function peaks corresponding to the production of Ar^+ ions in these two states. Hence, in this case, we were only able to show that found to $\beta_{m1}/\beta_{m3} = 2.1\pm 0.3$.

5.2. Ionization of carbon monoxide molecules

When metastable atoms collide with CO molecules at thermal energies, the only recorded ionization process is Penning ionization:

$$He(2^3S)+CO\rightarrow He+CO^{+}+e, \qquad (5.5)$$

$$He(2^1S)+CO\rightarrow He+CO^{+}+e. \qquad (5.6)$$

The quenching constant k_{m3} of $He(2^3S)$ atoms in collisions with CO at $T_a=300$ K is $k_{m3}=(16\pm3)\times10^{-11}$ cm^3 s^{-1} (this is an average over the nine available published results).

A more accurate result is obtained by averaging the data reported in Refs. 50–54 in which the most reliable methods were employed, namely, continuous afterglow and pulsed radiolysis. In this case, $k_{m3}=(10.0\pm0.6)10^{-11}$ cm^3 s^{-1}. The qunenching constant k_{m1} was measured in Refs. 50 and 55 for $He(2^1S)$. These two sets of data differ by a factor of two but the ratio of the 2^1S and 2^3S quenching constants is the same (3.2 ± 0.3 and 3.3 ± 0.6). Hence, the quenching constant of the $He(2^1S)$ atom turns out to be $k_{m1}=(32\pm4)\times10^{-11}$ cm^3 s^{-1}.

The energy dependence of the cross sections for reactions (5.5) and (5.6) was reported in Ref. 56. An absolute measure can be obtained for this dependence by normalizing to the quenching constants given in Ref. 50, which are practically identical with the above average data for CO. The absolute (without normalizing to the quenching constants) cross sections were measured in Refs. 57–59 at the fixed energies of 30, 40, and 140 meV, respectively. The difference between these values and the values reported in Ref. 56 ranges from 30% to a factor of 3 in the case of the 2^3S states and from 40% to a factor of 2 for the 2^1S states. This spread is a consequence of the considerable systematic uncertainty in the beam method, which arises from the calibration of the equipment.

Apart from reactions (5.5) and (5.6), the other processes that can occur in thermal collisions are

$$He(2^3S)+CO\rightarrow He+C+O, \qquad (5.7)$$

$$He(2^1S)+CO\rightarrow He+C+O. \qquad (5.8)$$

The excess energy, i.e., 8.7 eV in the first case and 9.5 eV in the second, can be expended in exciting the atoms. The rate constant for reaction (5.7) with the production of C^* atoms with an excitation energy of 7.5–7.9 eV, was measured in Refs. 60 and 61. The total probability of dissociation of CO with the excitation of these levels was found to be low and, according to the more accurate data given in Ref. 61, amounted to 2%. According to the authors of Ref. 61, the remaining 98% are used up in Penning ionization.

Precisely because the branching ratio η_{m3} for reaction (5.5) was close to unity, it was possible to normalize the cross section for reaction (5.5), obtained in Ref. 56, to the quenching constant of the $He(2^3S)$ atom [this was done for (5.6) although the information about the branching ratio η_{m1} is not available in this case].

It is important to note that, in addition to the C^* levels investigated in Refs. 60 and 61, energy considerations allow the possibility of the population of lower-lying metastable states of C and also of O in reaction (5.7). It may also be considered that low-lying C and O levels may become excited simultaneously, e.g., the $^5S_2^0$ states of C and the $^1S_0$ states of O with total energy of 8.4 eV. The question of the rate constant for reaction (5.7) and, consequently, for reaction (5.5) as well, cannot be considered as finally settled. Even more so, this applies to processes involving $He(2^1S)$ atoms because energy considerations allow the excitation of a larger number of levels of C^* and O^* in (5.8) than in (5.7), including levels close to resonance.

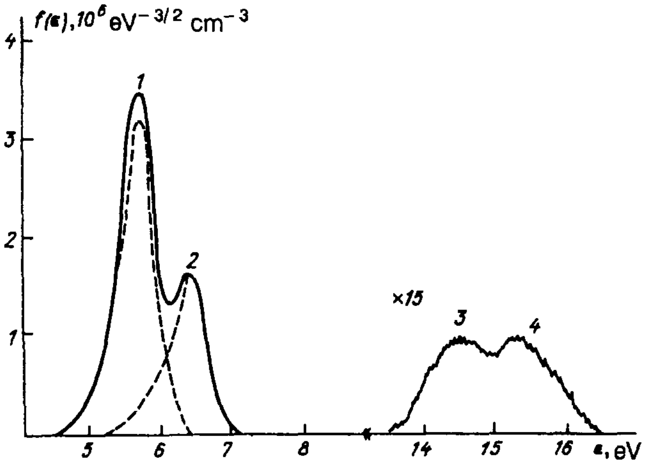

FIG. 7. High energy part of the distribution function in the helium +carbon monoxide mixture with a low percentage concentration of CO.

The first direct PES measurements of the rate constants of (5.5) and (5.6) were reported in Ref. 62. They were performed on the gas mixture He+0.1 CO at a pressure of 0.5 torr (the total impurity concentration did not exceed $5\times10^{-4\%}$ according to chemical and spectral analyses). The gas micture was continuously flushed through the system in order to exclude cataphoresis and to remove the products of plasmochemical reactions from the discharge. A pulsed periodic discharge with a 70-μs active phase and a period of 500 μs was initiated in a tube with an internal diameter of 2.3 cm. The distribution function was measured at intervals of 20–150 μs after the end of the discharge pulse (time resolution 5 μs).

Figure 7 shows a typical distribution function in the energy ranges in which the chemoionization reaction was significant. The characteristic peaks correspond to the following reactions:

$$He(2^3S)+CO\rightarrow CO^{+}(X^2\Sigma)+He+e(5.8\ \text{eV}), \qquad (5.9)$$

$$He(2^1S)+CO\rightarrow CO^{+}(X^2\Sigma)+He+e(6.5\ \text{eV}). \qquad (5.10)$$

The peaks at 14.4 and 15.4 eV are due to the reactions considered earlier and involving two triplet and triplet and singlet metastable helium atoms for which the rate constants are well known. The distribution function for this region was used to monitor the accuracy with which the fast-electron concentration and the concentration of metastable atoms were measured under the particular experimental conditions.

To separate the contributions of reactions (5.9) and (5.10), it was considered, in accordance with Ref. 63, that the widths of their spectra could be neglected in comparison with collisional broadening and the instrumental function of the detection system (0.2 V at half height). The following values were obtained: $\beta^{(X)}_{m3}=(0.5\pm0.1)\times10^{-10}$ $cm^3\,s^{-1}$ for reaction (5.9) and $\beta^{(X)}_{m1}=(1.1\pm0.2)\times10^{-10}$ $cm^3\,s^{-1}$ for reaction (5.10).

The large energy width ($\sim$2 eV) reported in Ref. 63 for the spectra from the reactions $He(2^{1,3}S)+CO\rightarrow CO^+(A^2\Pi)+He+e(2.5\text{–}4\ eV)$ and the rapid increase in the second derivative of the ion current at probe potentials below 4 V prevented a precise determination of the corresponding constants. For the reaction involving $He(2^3S)$, it was found that $\beta^{(A)}_{m3}=(0.15\pm0.06)\times10^{-10}$ $cm^3\,s^{-1}$. The process $He(2^{1,3}S)+CO\rightarrow +CO^+(B^2\Sigma)+He+e(1{,}0.2\ eV)$ was not recorded because the region in which the electrons were produced in this reaction contained a large number of Maxwellian electrons from the main group.

The relative yields of CO^+ ions in the $X^2\Sigma^+_g$, $A^2\Pi_u$, and $B^2\Sigma^+_u$ states in reactions (5.5) and (5.6), reported in Ref. 61 and 63–65, were used to determine the total rate constants for Penning ionization in the case of reaction (5.5). The results for (5.5) and (5.6) were $\beta_{m3}=(9\pm2)\times10^{-11}$ $cm^3\,s^{-1}$ and $\beta_{m1}=(2.4\pm0.6)\times10^{-10}$ $cm^3\,s^{-1}$, respectively. Accordingly, the values of η_{m3} and η_{m1} were found to $\eta_{m3}=9^{+0.1}_{-0.2}$, $\eta_{m1}=0.8\pm0.2$, and $\eta_{m1}/\eta_{m3}=0.85\pm0.15$.

It follows from these data Penning ionization is the principal channel for the quenching of metastable helium atoms by CO molecules. For the $He(2^3S)$ atoms, this is in agreement with Refs. 60 and 61. It is also in agreement with Refs. 66 where it was found that the probability of Penning ionization in collisions between all the above molecules and $He(2^3S)$, was greater than 0.6 whereas for diatomic molecules it was 0.7. Analogous results have not been available for clissions with $He(2^1S)$.

The above data show that the PES method can be used to determine the absolute rate constants for Penning ionization, using only simple and very precise calibration procedures. The uncertainty in the data obtained in this way can be reduced to 20 to 30% which is close to the uncertainties in modern methods of measuring the quenching constants of metastable atoms. The values obtained in this way can then be used to normalize the energy dependence of the cross sections for Penning ionization (and, in general, chemoionization). This seems more reasonable than normalization to the quenching constants because it does not involve the assumption that the ionization branching ratios are equal to unity.

Moreover, the values of η_m obtained from the comparison of ionization and quenching constants are accurate to 25–30%. The methods reported in previous publications[66,67] are subject to comparable or greater uncertainty (up to 100% in Ref. 66), and actually give only the relative value, so that a calibration relying on standard processes with precisely known constants or values of η has to be used to obtain the absolute values.

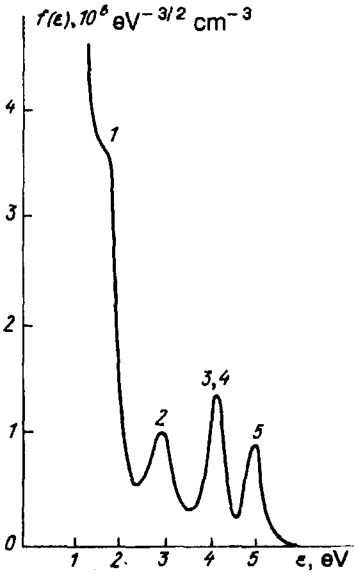

FIG. 8. Electron velocity distribution in the helium-nitrogen mixture in the region of the Penning ionization spectrum at low nitrogen concentration. The peaks are due to the following reactions, respectively: *1*—(5.16), *2*—(5.13), *3*—(5.11), *4*—(5.14) *5*—(5.12).

5.3. Ionization of nitrogen molecules

Since the CO and N_2 molecules have a similar structure, the ionization of these molecules by metastable helium atoms exhibits some common features.

We recall that PES studies of Penning ionization must be conducted in a mixture with a low ($\sim$0.1%) concentration of the molecular gas because the lifetime of the metastable atoms decreases with increasing concentration of the molecules, and the relation between the distribution function and the initial electron spectrum becomes more complicated (because the relaxation parameter can become equal to unity). Since we did not have our disposal calibrated He-N_2 mixtures, we were not able to flush the mixture through the system and to monitor the N_2 concentration with sufficient precision because of the rigidity effect. The PES method was therefore used only to find the ratio of the reaction rates, which is independent of the nitrogen pressure in this region. At the same time, the reliability of these results is enhanced by the fact that they rely on relative measurements.

Figure 8 shows a typical distribution function obtained[68] under the following conditions: helium pressure 0.4 torr, nitrogen pressure 3×10^{-4} torr, current per discharge pulse 8 mA, delay time 75 μs, discharge repetition frequency 2.8 kHz. The concentration of 2^1S and 2^3S metastable helium atoms was 3.1×10^{10} and 8.6×10^{10} cm^{-3}, respectively.

By analogy with He-Co mixture, the following reactions can occur in this mixture:

$$\mathrm{He}(2^3\mathrm{S})+\mathrm{N}_2\rightarrow\mathrm{He}+\mathrm{N}_2^+(\mathrm{X}^2\Sigma)+\mathrm{e}(4.2\ \mathrm{eV}),\qquad(5.11)$$

$$\mathrm{He}(2^1\mathrm{S})+\mathrm{N}_2\rightarrow\mathrm{He}+\mathrm{N}_2^+(\mathrm{X}^2\Sigma)+\mathrm{e}(5\ \mathrm{eV}),\qquad(5.12)$$

$$\mathrm{He}(2^3\mathrm{S})+\mathrm{N}_2\rightarrow\mathrm{He}+\mathrm{N}_2^+(\mathrm{A}^2\Pi)+\mathrm{e}(3.1\ \mathrm{eV}),\qquad(5.13)$$

$$\mathrm{He}(2^1\mathrm{S})+\mathrm{N}_2\rightarrow\mathrm{He}+\mathrm{N}_2^+(\mathrm{A}^2\Pi)+\mathrm{e}(3.9\ \mathrm{eV}),\qquad(5.14)$$

$$\mathrm{He}(2^3\mathrm{S})+\mathrm{N}_2\rightarrow\mathrm{He}+\mathrm{N}_2^+(\mathrm{B}^2\Sigma)+\mathrm{e}(0.9\ \mathrm{eV}),\qquad(5.15)$$

$$\mathrm{He}(2^1\mathrm{S})+\mathrm{N}_2\rightarrow\mathrm{He}+\mathrm{N}_2^+(\mathrm{B}^2\Sigma)+\mathrm{e}(1.8\ \mathrm{eV}).\qquad(5.16)$$

Reaction (5.15) is difficult to record by the PES method because the Maxwellian tale of the distribution function is significant in this energy range. Reaction (5.16) appears as a singularity on the rapidly rising ion current background. The spectrum from reaction (5.14) is relatively broad because of the contribution due to transitions between different vibrational levels. The energies and the branching ratios corresponding to the different states of the N_2^+ ions in the recorded reactions are in agreement, to within the experimental uncertainty, with the data reported in Ref. 65, 69, and 70. Reactions (5.11) and (5.16) were investigated earlier, mainly by Penning spectroscopy S^{10} and by measuring the fall in the $\mathrm{He}(2^{3,1}\mathrm{S})$ concentration in continuous afterglow.[50] The advantages and disadvantages of these methods have already been discussed.

The quenching constants of metastable triplet atoms are well known, and the average evaluated over a large number of published data is $k_{\mathrm{m3}}=7.1\pm0.110^{-11}\ \mathrm{cm}^3\mathrm{s}^{-1}$ (Ref. 19). As far as the corresponding constant for $\mathrm{He}(2^3\mathrm{S})$ is concerned, we know of only one publication in which k_{m1} was determined with considerable uncertainty:[50] $k_{\mathrm{m1}}=(17\pm5)\times10^{-11}\ \mathrm{cm}^3\,\mathrm{s}^{-1}$. According to Ref. 61, the principal channel for the quenching of metastable helium atoms by nitrogen molecules is Penning ionization (which is in agreement with earlier data on the CO molecule). Consequently, PES measurements with known branching ratios for the (5.11)–(5.16) reactions[65,69,70] can be used to obtain accurate values such as $\beta_{\mathrm{m1}}=\beta_{\mathrm{m3}}=(2.1\pm0.4)$ and to reduce the uncertainty in k_{m1} indicated in Ref. 50. The final result is $k_{\mathrm{m1}}=(15\pm3)\times10^{-11}\ \mathrm{cm}^3\,\mathrm{s}^{-1}$.

We note that, at least in principle, PES can be used under such conditions to investigate Penning reactions between metastable atoms and molecules in excited electronic states, for example,

$$\mathrm{He}(2^{3,1}\mathrm{S})+\mathrm{N}_2(\mathrm{A}^3\Sigma)\rightarrow\mathrm{He}+\mathrm{N}_2^++\mathrm{e},\qquad(5.17)$$

for which there are no published data. In accordance with Ref. 71, the relative fraction of electronically-excited molecules in the plasma of the helium mixture with a small concentration of nitrogen can amount to a few per cent of the concentration of normal molecules. The spectrum of a reaction similar to (5.17) was recorded when the distribution function was obtained in the energy range 7–11 eV, but, to obtain quantitative data, it is essential to flush the mixture through the system whilst measuring the concentration of $\mathrm{N}_2\mathrm{A}^3\Sigma$ molecules by optical methods.

6. QUENCHING OF EXCITED INERT-GAS AND MERCURY ATOMS BY ELECTRONS

This part of our review is devoted to reaction (1.3) which was investigated by the method described above in the electron-temperature range $300\leqslant T_{\mathrm{e}}\leqslant3000$ K in inert-gas and mercury plasma afterglow. We beging by noting its advantages in studies of quenching reactions. First, it is a direct method because the rate constant $\beta_{\mathrm{e}}(T_{\mathrm{e}})$ for the process is determined directly from the resulting particles, i.e., fast electrons. Second, by using the second pulse to produce additional heating of the electron gas,[15] we can determine the temperature dependence $\beta_{\mathrm{e}}(T_{\mathrm{e}})$ and then use it to examine the excitation and de-excitations cross sections near the threshold. By definition, the rate constant for (1.3) is related to the quenching cross section $\sigma_2(\varepsilon)$ by the expression $\beta_{\mathrm{e}}(T_{\mathrm{e}})=\langle\sigma_2(\varepsilon)v(\varepsilon)\rangle$ where $v(\varepsilon)$ is the velocity of an electron with energy ε, and the average is evaluated over the Maxwellian distribution of electrons at temperature T_{e}. The excitation cross section σ_1 is related to σ_2 through the principle of detailed balancing:[19] $\sigma_2(\varepsilon)\varepsilon g_{\mathrm{m}}=\sigma_1(\varepsilon_1+\varepsilon)(\varepsilon_1+\varepsilon)g_{\mathrm{a}}$. According to the theory given in Ref. 72, the dependence of σ_1 on the energy of electrons near the excitation threshold has a root-type character, and $\beta_{\mathrm{e}}(T_{\mathrm{e}})=\mathrm{const}$. However, the presence of energy levels corresponding to the formation of a negative ion can modify this dependence and may lead to a nonmonotonic behavior of $\sigma_1(\varepsilon)$ (Ref. 73). The apperance of resonances complicates the theoretical determination of $\sigma_1(\varepsilon)$ near the threshold and, as far as we know, the only reported inert-gas calculations of this kind are those described in Refs. 74 and 75 for helium and neon.

Experiments in which the scattering of an electron beam by atoms in the ground or metastable states was investigated (see, for example, Refs. 76 and 77) have produced a considerable volume of data, but, in most cases, the energy spread in the electron beam was 0.5–0.7 eV, which means that these results cannot be used to determine the behavior of $\sigma_1(\varepsilon)$ in the near-threshold energy range in which we are interested here. Recent years have seen considerable advances in beam methods[78–82] which have resulted in a substantial reduction in the electron energy spread in the exciting beam. For example, this spread was 35–50 meV in Refs. 78 and 4.88–9.71 meV in Refs. 79 and 80. However, the apparatus used in these experiments[78–81] was not good enough for measurements of the absolute excitation cross sections. Absolute differential excitation cross sections were obtained in Ref. 82 for the $4p^5s$ levels of krypton, using an electron-energy spread of 33–35 meV, but only for three scattering angles.

The foregoing discussion shows that measurements of $\beta_{\mathrm{e}}(T_{\mathrm{e}})$ at low electron temperatures would be highly desirable.

6.1. Helium

The absolute value and the temperature dependence of the rate constant $\beta_{\mathrm{e}}(T_{\mathrm{e}})$ for the reaction

$$\mathrm{He}(2^3\mathrm{S})+\mathrm{e}\rightarrow\mathrm{He}(^1\mathrm{S}_0)+\mathrm{e}\qquad(6.1)$$

were determined in Ref. 83 from the peak on the distribu-

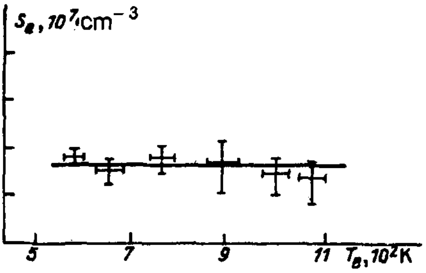

FIG. 9. S_e as a function of T_e in helium.

tion function at $\varepsilon_1 = 19.8$ eV. It is clear from existing data[23,84,85,87-90] on the constant β_e that there is a significant discrepancy between the absolute values of this constant and its dependence on electron temperature. Let us consider the temperature dependence in greater detail. In the most frequently cited experimental paper,[88] the excitation of helium by electron impact was investigated by using secondary-electron detection to determine $\sigma_1(\varepsilon)$. The initial part of the resulting curve for the excitation of the metastable 2^3S_1 state has been used by a number of workers to find $\sigma_2(\varepsilon)$ and $\beta_e(T_e)$. The results of these calculations depend significantly on which particular approximation was used to fit the experimental curve from Ref. 88. Some workers[23,85] assume that $\sigma_1(\varepsilon) \sim \varepsilon - \varepsilon_1$ for $\varepsilon - \varepsilon_1$ less than a few tenths of eV, and find that $\sigma_2 = \text{const}$ and $\beta_e \sim T_e^{1/2}$. Others[89] assume that $\sigma_1(\varepsilon) \sim (\varepsilon - \varepsilon_1)^{1/2}$ and find that $\sigma_2 \sim \varepsilon^{-1/2}$, $\beta_e = \text{const}$. In our view, the experimental data reported in Ref. 88 cannot be used to establish unambiguously the temperature dependence of β_e for $T_e \leqslant 2000$ K, i.e., for temperatures most often encountered in afterglow, since the electron energy spread in the exciting beam was 0.1 eV. It is probably also difficult to establish the character of this dependence by investigating the breakup of the 2^3S state in afterglow as was done, for example, in Ref. 90. In this case, several plasma parameters (N_e, N_m, T_e) must be measured simultaneously with high precision in order to obtain reliable results.

The precision with which the temperature dependence of β_e is determined can be substantially improved by using the following method. It is clear from (2.5) that β_e is proportional to S_e at constant N_m and N_e. Consequently, the function $\beta_e(T_e)$ can be obtained by varying T_e between certain limits in a particular afterglow phase. This is done by applying a second delayed voltage pulse to the electrodes of the discharge tube,[15] which produces a weak electric field that increases the temperature T_e, but does not affect N_m or N_e.

Figure 9 shows the measured values of S_e, obtained under the following conditions: helium pressure 0.8 torr, main pulse current 1.2 A, delay of second pulse 350 μs. The current and the electric field in the second pulse were varied from 5 to 35 mA and from 6 to 34 mV/cm, respectively. The constancy of the concentration of metastable atoms when the current in the second pulse was varied was monitored by measuring the area under the peak on the distribution function at 14.4 eV, which is proportional to N_m^2. The concentration of metastable atoms was found to remain constant to within 5%. It is clear from Fig. 9 that, for electron temperatures in the range 550–1100 K, the quantity S_e and, consequently, β_e too, were constant to within 10%. The fact that β_e was temperature-independent for $T_e \leqslant 1000$ K is also indicated by theoretical calculations[75,89] and the experimental results.[84] The magnitude of β_e was calculated from (2.5) and was found to be $\beta_e = (3.1 \pm 0.6) \times 10^{-9}$ cm^3 s^{-1}. This result is closest to Refs. 84, 75, and 89, i.e., $(4.2 \pm 0.6) \times 10^{-9}$ cm^3 s^{-1}, $(2.9 \pm 0.6) \times 10^{-9}$ cm^3 s^{-1}, and $(4.5 \pm 1.0) \times 10^{-9}$ cm^3 s^{-1}, respectively, and agrees with the figure of $(2.8 \pm 1.0) \times 10^{-9}$ cm^3 s^{-1} reported in Ref. 19.

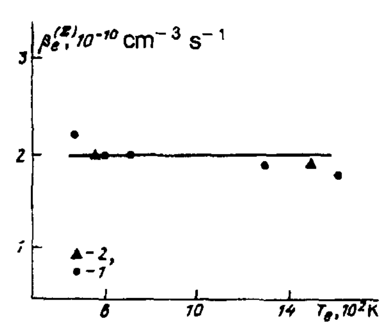

FIG. 10. Rate constant $\beta_e^{(\Sigma)}$ as a function of temperature in neon: 1—pressure 0.9 torr, $N_m^{(2)} = 3.2 \times 10^{11}$ cm^{-3}, $N_e = 1.6 \times 10^{11}$ cm^{-3}, $S_e^{(\Sigma)} = 7 \times 10^5$ cm^{-3}, 2—pressure 1.4 torr, $N_m^{(2)} = 3.5 \times 10^{11}$ cm^{-3}, $N_e = 1.7 \times 10^{11}$ cm^{-3}, $S_e^{(\Sigma)} = 10^6$ cm^{-3}.

6.2. Neon and argon

The reactions

$$\mathrm{Ne}(2p^5\ 3s\ {}^3P_2) + e \rightarrow \mathrm{Ne}(2p^6\ {}^1S_0) + e, \tag{6.2}$$

$$\mathrm{Ar}(3p^5\ 4s\ {}^3P_2) + e \rightarrow \mathrm{Ar}(3p^6\ {}^1S_0) + e \tag{6.3}$$

were investigated by using the distribution-function peaks at 16.6 and 11.5 eV, respectively.[14,24] Since four reactions with the participation of atoms in the ${}^3P_{0,1,2}$ and ${}^1P_1$ electronic states are possible in the neon and argon afterglow, the corresponding reaction rates will be denoted by $\beta_e^{(k)}$ where $k = 0,1,2,3$ refer atoms in the ${}^3P_0$, ${}^3P_1$, ${}^3P_2$, and ${}^1P_1$ states, respectively. As far as we know, prior to the publication of Refs. 14, 24, 27, and 28, there were no published data on direct measurements of these constants at electron energies $\varepsilon < 1$ eV.

Since the sublevel separation in the above configuration is in the range 0.05–0.13 eV, and the amplitude of the differentiating signal is about 1 V, the quantity $S_e^{(\Sigma)} = \Sigma S_e^{(k)}$ determined from the distribution function is the resultant for all four possible reactions. Consequently, the constant $\beta_e^{(\Sigma)}$ found from $S_e^{(\Sigma)}$ is an effective constant.

The results obtained by analyzing the experimental data for neon are shown in Fig. 10.

Theory predicts[74,91] that the rate constants for collisions of the second kind with the participation of atoms in the ${}^3P_2$, ${}^3P_1$, ${}^3P_0$, and ${}^1P_1$ states have very similar values. Moreover, our experiments have shown that

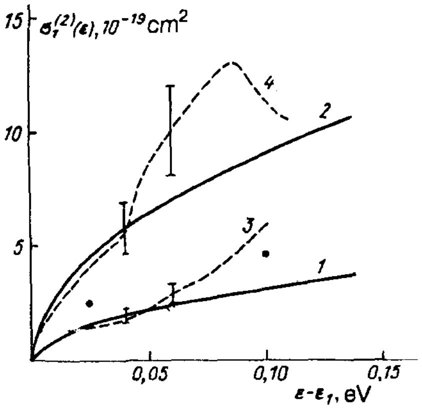

FIG. 11. Cross section for collisions of the first kind as a function of energy for the $^3P_2$ level in the near-threshold region: *1*, *2*—results from Ref. 14 and 24, for neon and argon, respectively, *3*, *4*—results of beam experiments,[79] in neon and argon, respectively; calculations for neon taken from Ref. 74.

$N_m^{(1)}/N_m^{(2)} \leqslant 0.25$, $N_m^{(0)}/N_m^{(2)} \leqslant 0.05$, and $N_m^{(3)}/N_m^{(2)} \leqslant 0.01$. It was therefore assumed that the effective constant $\beta_e^{(\Sigma)}$ obtained as described above was the reaction constant $\beta_e^{(2)}$ for (6.2) and (6.3). Our results show that the constant $\beta_e^{(2)}$ for neon is temperature independent to within ±15% at temperatures in the range $T_e = 4.70$–1700 K. Its value in this range is $\beta_e^{(2)} = (2.0 \pm 0.3) \times 10^{-10}$ cm^3 s^{-1}. In argon, we again have a constant result to within ±20% in the temperature range $T_e = 800$–1500K, namely, $\beta_e^{(2)} = (2.0 \pm 0.3) \times 10^{-10}$ cm^3 s^{-1}. The following values were reported in Refs. 27 and 28 at mean electron energy of 0.6 eV: $\beta_e^{(2)} = (2.7 \pm 0.5) \times 10^{-10}$ cm^3 s^{-1} in neon and $\beta_e^{(2)} = (2.8 \pm 0.4) \times 10^{-10}$ cm^3 s^{-1} in argon.

The lowest energy spread in the electron beam used to investigate inert-gas excitation was achieved in Ref. 79. However, even these results do not allow us to calculate the function $\beta_e^{(2)}(T_e)$ for neon and argon in a wide range of electron temperatures and then to compare the results with the abovevalues. The point is that Ref. 79 gives the behavior of the resultant excitation cross section for the two metastable states $^3P_2$ and $^3P_0$ in relative units, and since the energy separation between these states is 0.09 eV in neon and 0.17 eV in argon, this restricts possible calculations of $\beta_e^{(2)}(T_e)$ to temperatures $T_e \leqslant 600$ K in neon and $T_e \leqslant 800$ K in argon. The lower temperature limit is then 300–400 K and is determined by the energy spread in the beam. We shall therefore confine our attention to the behavior of the excitation cross section for the $^3P_2$ state in the near-threshold region. Our results showe that this cross section is $\sigma_1^{(2)} \sim (\varepsilon - \varepsilon_1)^{1/2}$ and it is important to remember that the cross section data deduced from measurements of $\beta_e^{(2)}$ is an integrated result that is insensitive to the fine structure of this function.

Figure 11 shows $\sigma_1^{(2)}(\varepsilon) \sim (\varepsilon - \varepsilon_1)^{1/2}$ calculated from the measured constants $\beta_e^{(2)}$ and also the function $\sigma_1^{(2)}(\varepsilon)$ from Ref. 79, both calibrated to give them their absolute values. The calibration was based on our constants at $T_e = 700$ K in neon and $T_e = 800$ K in argon.

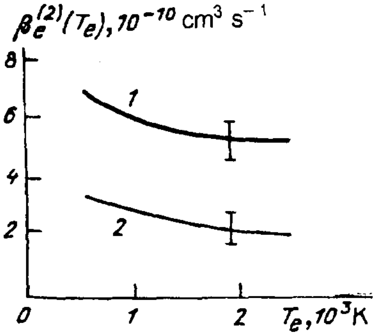

FIG. 12. Temperature dependence of rate constants for collisions of the second kind between electrons and Xe($^3P_2$) atoms (curve *1*) and Kr($^3P_2$) atoms (curve *2*).

6.3. Krypton and xenon

The following two points were taken into consideration when heavy inert gases were investigated experimentally. First, the excitation of normal atoms in the $^3P_2$ and $^3P_1$ states by fast electrons provides a greater contribution in krypton than xenon. The result is a reduction in the number $S_e^{(2)}$ of fast electrons in the peak on the distribution-function in which we are interested (9.9 eV in krypton and 8.3 eV in xenon) at electron temperatures $T_e > 600$ K, and the relation between $S_e^{(2)}$ and $\beta_e^{(2)}$ becomes more complicated. Second, the separation between the metastable $^3P_2$ and $^3P_0$ states is greater than in the lighter inert gases, and amonts to 0.65 eV in krypton and 1.14 eV in xenon, which means that it is possible to construct the function $\beta_e^{(2)}(T_e)$ from beam data[79] at temperatures $500 \leqslant T_e \leqslant 2000$ K in relative units. We therefore proceeded as follows. PES was applied to the plasma afterglow to determine the rate constants for collisions of the second kind between slow electrons and metastable krypton and xenon atoms in $^3P_2$ states at $T_e = 600$ K (the concentration of atoms in other excited states was negligible). The values of these constants were found to be $\beta_e^{(2)} = (3.4 \pm 0.5) \times 10^{-10}$ cm^3 s^{-1} for krypton and $\beta_e^{(2)} = (6.9 \pm 0.7) \times 10^{-10}$ cm^3 s^{-1} for xenon.

The function $\beta_e^{(2)}(T_e)$ was then constructed in relative units from the data reported in Ref. 79 and was calibrated against the above results at $T_e = 600$ K. The resulting curves are shown in Fig. 12. The magnitude of $\beta_e^{(2)}$ then allowed us to construct, on an absolute scale, the functions $\sigma_1^{(2)}(\varepsilon)$ from Ref. 79. The corresponding curves are shown in Fig. 13.

The values of the rate constants for the quenching of metastable atoms by slow electrons in inert gases are listed in Table V.

6.4. Mercury

Studies of quenching in mercury afterglow have shown that the rate constant for the de-excitation of the metastable $^3P_2$ state by electron impact is significantly greater than the corresponding result for inert gases. The result for $T_e = 2000$ K is $\beta_e^{(2)} = (2.9 \pm 1.2) \times 10^{-8}$ cm^3 s^{-1}. This is related to the sharp rise in the cross section for the excitation of the $^3P_2$ state directly at the threshold, which can be

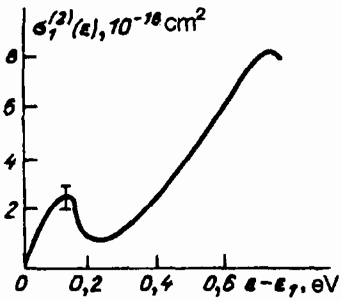

FIG. 13. Excitation of the $^3P_2$ level in xenon.

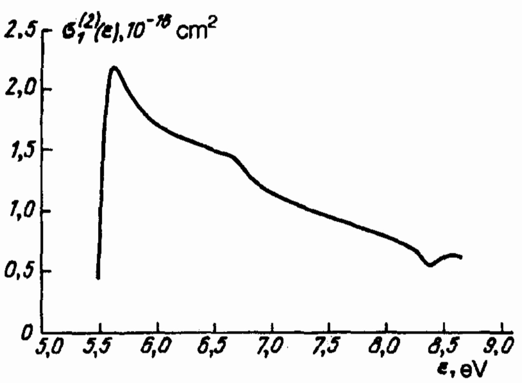

FIG. 14. Excitation of the $^3P_2$ level in mercury.

seen in Fig. 14. We use the above reaction rate constant to calibrate this curve, which was reported in Ref. 92. The cross section at the $\varepsilon = 5.6$ eV peak is 2.2×10^{-16} cm^2, which is somewhat lower than the measured cross section reported in Ref. 93 (3.2×10^{-16} cm^2) and the calculated value given in Ref. 94 (3×10^{-16} cm^2).

7. EFFECT OF FAST ELECTRONS ON PLASMA PORPERTIES

The above results show that the reactions (1.1)–(1.3) can play an important part in the de-excitation of atoms and the production of electrons, atomic ions, and molecular ions. Since plasma is a system with a mutually dependent parameters, these reactions must influence other processes, e.g., stepwise excitation, evolution of electron temperature, and so on. Naturally, (1.1)–(1.3) provide different contributions under different experimental conditions and, in each case, must be specifically taken into account in so far as they influence the plasma parameters. A detailed analysis of the possible effect of these reactions on plasma properties is given in the review paper in Ref. 6. Here, we shall confine our attention to a brief summary of the questions that are particularly interesting from our point of view.

It is shown in Refs. 95 and 96 that the contribution of reactions (1.1)–(1.3) rises substantially whenever the so-called continuous electron spectrum is present at energies between the fast-electron appearance energy and a few tenths of eV. For $\varepsilon \gg T_e$, the continuous electron spectrum is due to the change in the boundary conditions for fast electrons. These electrons usually escape to the walls by free diffusion and experience almost no elastic reflection at the walls.[95] It is precisely this case that was examined in Section 2 when we calculated the distribution function. However, the free diffusion process comes to an end when the diffusion parameter P, i.e., the ratio of the number of fast electrons, created per unit tube length per unit time, to the number of ions, escaping to the walls by ambipolar diffusion, is greater than unity. Some of the fast electrons must be retained within the volume of the tube if the quasineutrality condition is to be met for $P > 1$. This is achieved by increasing the potential difference near the wall from a few kT_e/e to a value corresponding to the electron appearance energy in reactions (1.1)–(1.3). As a result, some of the fast electrons whose energy is insufficient to overcome the potential difference near the wall are trapped within the volume, and their departure from this energy range is determined by the effectiveness of elastic electron-atom and electron-electron collisions. The final result of all this is the appearance of a continuous electron spectrum.

TABLE V. Rate constants for the quenching of metastable atoms by slow electrons in inert gases.

Metastable atoms	β_e, 10^{-10} cm^3 s^{-1}	Dependence of β_e on T_e	Range of variation of T_e, K
He(2^3S)	31 ± 6	Const	550 — 1100
Ne($^3P_2$)	2,0 ± 0,3	Const	470 — 1600
Ar($^3P_2$)	4,0 ± 0,8	Const	800 — 1500
Kr($^3P_2$)	3,4 ± 0,5	see *Fig. 12*	600
Xe($^3P_2$)	6,9 ± 0,7	» »	600

We note that, prior to the publication of Ref. 95, there were discussions of the effect of the shape of the distribution function on the potential difference Φ near the wall. For example, it was shown in Ref. 97 that diffusion to the discharge-tube walls can produce a depletion of the distribution function for energies of the order of a few keV, thus reducing Φ. However, the change in Φ produced by intensive activity associated with reactions (1.1)–(1.3) is significantly different from that discussed in Ref. 97 both qualitatively (in the sense of the cause of the phenomenon) and quantitatively (when the continuous spectrum appears, Φ increases and, depending on the gas and the prevailing conditions, can reach values of 4–20 eV, whereas the change in Φ due to diffusional depletion of the distribution function in afterglow plasma amounts to a few tenths of eV and leads to a reduction in the absolute value of Φ).

The onset and evolution of this interesting phenomenon has been observed[98] in the afterglow plasma of inert gases. For example, Fig. 15 shows the fast part of the electron distribution function, measured in xenon (pressure 0.2 torr, current 5 mA). A transition from free diffusion ($P < 1$) to an anomalously large jump in potential ($P > 1$) is eventually observed. One can clearly see the evolution of the continuous electron spectrum for energies $\varepsilon \leqslant 4.5$ eV, which agrees with the above analysis. Figure 16

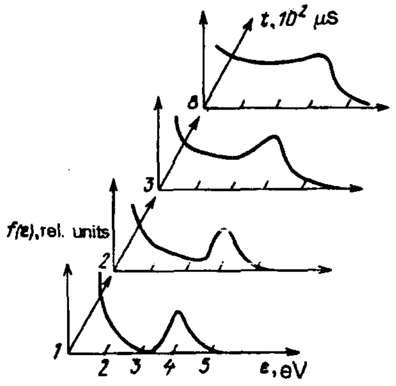

FIG. 15. Electron velocity distribution in the afterglow plasma in xenon at different afterglow times.

shows measurements and calculations of the potential Φ under the same conditions. It is clear that the appearance of the fast electrons results in an agreement between calculations and measurements. The continuous spectrum leads, in turn, to the effective heating of the slow Maxwellian electrons by fast electrons, which must be taken into account in calculations of T_e. For the same conditions in the afterglow plasma, there is an increase in the contribution of stepwise excitation and ionization, slow electrons cease to escape to the tube walls, and there is no diffusional cooling of these electrons.[6,96]

The conditions necessary for the appearance of the continuous electron spectrum can also be created artificially by applying a regulated trapping potential to the tube walls and thus controlling the optical and electrical parameters of the plasma.[86]

We also note that the effects associated with the appearance of the potential jump $\Phi \gg kT_e$ near the wall can be observed not only in current-free plasma but also under other conditions when groups of fast electrons are produced in plasmas (pinched discharges, stratified discharges, steady low-current discharges).

CONCLUSIONS

It is clear from the foregoing discussion that the utilization of existing experimental methods has produced extensive data on ionization and quenching processes with the participation of excited atoms.

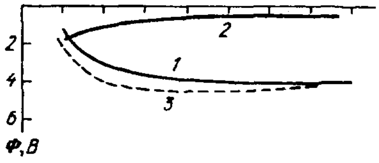

FIG. 16. Jump in potential near the wall, Φ, in the afterglow plasma in xenon: *1*—experiment, *2*—calculation without fast electrons or the anomalous potential jump, *3*—with fast electrons.

Chemoionization involving two excited particles, especially in radiative states, is of particular interest from the point of view of practical applications and theoretical analyses. An increase in the number of publications is expected in this area, including publications reporting the application of laser excitation and de-excitation of particular levels.

The most complete and detailed information about the above processes will come from the combined application of different methods, including the mass spectrometer, Penning electron spectroscopy, and PES. This approach will exploit the advantages and reduce the relative disadvantages of these techniques. The volume of available information will have to expanded by increasing the sensitivity and resolution of experimental procedures. As far as the PES method is concerned, it will soon become possible to record plasma electron spectra with a resolving power of 30–50 meV and sensitivity of 10^4 cm^{-3}. Finally, the possibilities of PES can be extended by applying it to the plasma afterglow and to studies of chemoionization in cryogenic plasmas.

[1] R. H. Neynaber, *Proc. Eleventh Conference on the Physics of Electronic and Atomic Collisions*, Koyoto, 1979, p. 287.

[2] V. B. Leonas and A. P. Kalinin, Usp. Fiz. Nauk **121**, 561 (1977) [Sov. Phys. Usp. **20**, 779 (1977)].

[3] B. M. Smirnov, Usp. Fiz. Nauk **133**, 569 (1981) [Sov. Phys. Usp. **24**, 251 (1981)].

[4] N. B. Kolokolov, *Plasma Chemistry* in Russian, edited by B. M. Smirnov, Energoatomizdat, M., 1985, p. 56.

[5] A. N. Klyucharev and M. L. Yansons, *Elementary Processes in Alkali Metal Plasmas* [in Russian], Energoatomizdat, M., 1988.

[6] N. B. Kolokolov and A. A. Kudryatsev, *Plasma Chemistry* [in Russian], edited by B. M. Smirnov, Energoatomizdat, M., 1989, p. 127.

[7] N. V. Bedenkov, N. B. Kolokolov, A. A. Kudryavtsev *et al.*, Zh. Tekh. Fiz. **58**, 469 (1989) [Sov. Phys. Tech. Phys. **33**, 282 (1989)].

[8] N. B. Kolokolov, A. A. Kudryavtsev, and V. A. Romanenko, Zh. Tekh. Fiz. **56**, 1737 (1986) [**31**, 1033 (1986)].

[9] A. B. Blagoev, N. B. Kolokolov, and V. M. Milenin, Zh. Tekh. Fiz. **42**, 1701 (1972) [Sov. Phys. Tech. Phys. **17**, 1359 (1972)].

[10] S. E. Kupriyanov, and S. P. Kabanov, *Plasma Chemistry* [in Russian], edited by B. M. Smirnov, Energoatomizdat, M., 1976, p. 189.

[11] Yu. M. Kagan and V. I. Perel', Usp. Fiz. Nauk **81**, 409 (1973).

[12] G. M. Malyshev and V. L. Fedorov, Dok. Akad. Nauk SSSR **52**, 269 (1953).

[13] A. B. Blagoev, Yu. M. Kagan, N. B. Kolokolov *et al.*, Zh. Tekh. Fiz. **45**, 579 (1975) [eztf **20**, 360 (1975)].

[14] V. I. Demidov and N. B. Kolokolov, Zh. Tekh. Fiz. **48**, 1832 (1978) [Sov. Phys. Tech. Phys. **23**, 1044 (1978)].

[15] G. N. Gerasimov, R. I. Lyagushchenko, and G. P. Stratsev, Opt. Spektrosk. **30**, 606 (1971).

[16] S. E. Frish, *Spectroscopy of Gas-Discharge Plasmas* [in Russian], Nauka, L., 1970, p. 7.

[17] L. M. Volkova, V. I. Demidov, N. B. Kolokolov *et al.*, Zh. Tekh. Fiz. **53**, 913 (1983) [Sov. Phys. Tech. Phys. **28**, 583 (1983)].

[18] A. N. Tikhonov and V. Ya. Arsenin, *Methods of Solving Ill-Posed Problems* [in Russian]. Nauka, M., 1974.

[19] B. M. Smirnov, *Excited Atoms* [in Russian], Energoatomizdat, M., 1982.

[20] N. B. Kolokolov and P. M. Pramatarov, Zh. Tekh. Fiz. **48**, 294 (1978) [Sov. Phys. Tech. Phys. **23**, 176 (1978)].

[21] B. M. Smirnov, *Ions and Excited Atoms in Plasmas* [in Russian], Atomizdat, M., 1980.

[22] A. A. Radtsig and B. M. Smirnov, *Handbook on Atomic and Molecular Physics* [in Russian], Atomizdat, M., 1980.

[23] A. N. Soldatov, Opt. Spektrosk. **31**, 181.

[24] I. Yu. Baranov, V. I. Demidov, and N. B. Kolokolov, Izv. Vyssh. Uchebn. Zav., Fiz. No. 8, 117 (1982).

[25] Yu. Z. Ionikh, N. P. Penkin, and A. V. Samson, Vestn. Leningrad. Univ., Ser. Fiz. Khim. No. **10**, 50 (1974).

[26] A. Rutscher and S. Pfau, Beitr. Plasmaphys. No. 7, 187 (1967).

[27] A. B. Blagoev and T. K. Popov, Phys. Lett. A **66**, 210 (1978).

[28] A. B. Blagoev and T. K. Popov, Phys. Lett. A **70**, 416 (1979).

[29] N. B. Kolokolov and O. G. Toronov, Opt. Spektrosk. **55**, 434 (1983) [Opt. Spectrosc. (USSR) **55**, 254 (1983)]..

[30] N. B. Kolokolov and O. G. Toronov, *Proc. Nineteenth All-Union Conference on Spectroscopy* [in Russian], Pt. I, Tomsk, 1983, p. 285.

[31] N. B. Kolokolov and O. G. Toronov, *Proc. Sixth All-Union Conference on the Physics of Low-Temperature Plasmas* [in Russian], Pt. I, L., 1983, p. 23.

[32] A. B. Blagoev, T. M. Mishonov, and T. K. Popov, *Proc. International Conference on Phenomena in Ionized Gases,* Minsk, 1981, p. 381.

[33] A. B. Blagoev and T. K. Popov, *Proc. Tenth Jubilee National Conference on Atomic Spectroscopy,* Veliko Turnovo, Bulgaria, 1982, p. 108.

[34] M. Aymar and M. Coulomber, At. Data Nucl. Data Tables **21**, 537 (1978).

[35] W. L. Wiese and G. A. Martin, *Wavelengths and Transiton Probabilities for Atoms and Atomic Ions,* Pt. II, NSRDS-NBS, **68**, Government Printing Office, Washington DC, 1980, p. 359.

[36] B. J. Garrison, W. H. Miller, and H. F. Schaefer, J. Chem. Phys. **59**, 3193 (1973).

[37] A. Z. Devdariani, V. I. Demidov, N. B. Kolokolov *et al.*, Zh. Eksp. Teor. Fiz. **84**, 1646 (1983) [Sov. Phys. JETP **57**, 960 (1983)].

[38] W. H. Miller, J. Chem. Phys. **52**, 3563 (1970).

[39] H. O. Dickinson and M. R. H. Rudge, J. Phys. B **3**, 1448 (1970).

[40] J. S. Cohen and B. Schneider, J. Chem. Phys. **61**, 3230 (1974).

[41] M. W. Müller, A. Merz, M. W. Ruf *et al.*, Z. Phys. D **21**, 89 (1991).

[42] V. B. Borisov, V. S. Egorov, and N. A. Ashurbekov, *Proc. Sixth All-Union Conference on the Physics of Low-Temperature Plasmas* [in Russian], L., 1983, p. 20 (LIYaF Preprint).

[43] S. E. frish, *Optical Spectra of Atoms* [in Russian], Fizmatgiz, L.-M., 1983.

[44] H. Hotop and A. Niehaus, Z. Phys. **228**, 68 (1969).

[45] M. L. Coleman, R. Hammond, and J. W. Dubrin, Chem Phys. Lett. **19**, 271 (1973).

[46] F. Chermak, J. Electron. Spectrosc. Rel. Phen. **9**, 419 (1976).

[47] A. Le Nadan, G. Le Coz, F. Tuffin *et al.*, J. Phys. (Paris) **43**, 419 (1982).

[48] C. E. Brion, C. A. McDowell, and W. B. Stewart, J. Electron. Spectrosc. Rel. Phen. **1**, 113 (1972).

[49] A. G. Nikitin, Candidate Thesis [in Russian], St. Petersburg, 1992.

[50] A. L. Schmeltekopf and F. C. Fehsenfeld, J. Chem. Phys. **53**, 3173 (1970).

[51] R. C. Bolden, R. S. Hemsworth, M. J. Shaw *et al.*, J. Phys. B **3**, 61 (1970).

[52] F. W. Lee and C. B. Collins, J. Chem. Phys. **65**, 5189 (1976).

[53] T. Ueno, A. Yokoyama, S. Takao *et al.*, Chem. Phys. Lett. **45**, 261 (1980).

[54] H. Koizumi, M. Ukai, J. Tanaka *et al.*, J. Chem. Phys. **85**, 1931 (1986).

[55] Yu. Z. Ionikh, N. P. Penkin, and S. P. Yakovitskiĭ, Opt. Spektrosk. **66**, 1285 (1989) [Opt. Spectrosc. (USSR) **66**, 748 (1989)].

[56] T. P. Parr, D. M. Parr, and R. M. Martin, J. Chem. Phys. **76**, 316 (1982).

[57] W. R. Sholette and E. E. Muschlitz, J. Chem. Phys. **36**, 3368 (1962).

[58] W. P. West, T. B. Cook, F. B. Dunning *et al.*, J. Chem. Phys. **63**, 1237 (1975).

[59] P. A. Jerram and A. C. H. Smith, J. Phys. B **18**, 1747 (1985).

[60] W. B. Hurt and W. C. Grable, J. Chem. Phys. **57**, 734 (1972).

[61] R. S. F. Chang, D. W. Setser, and G. W. Taylor, Chem. Phys. Lett. **25**, 201 (1978).

[62] Yu. Z. Ionikh, N. B. Kolokolov, A. A. Kudryavtsev *et al.*, Opt. Spektrosk. **71**, 941 (1991) [Opt. Spectrosc. (USSR) **71**, 542 (1991)].

[63] Y. Harada, K. Ohno, and H. Mutoh, J. Chem. Phys. **79**, 3251 (1983).

[64] H. Hotop and A. Niehaus, Int. J. Mass. Spectrosc. Ion. Phys. No. 5, 415 (1970).

[65] D. S. C. Yee, W. B. Stewart, C. A. McDowell *et al.*, J. J. Electr. Spectrosc. relat. Phen. 7, 93 (1975).

[66] M. T. Jones, T. D. Dreiling, D. W. Setser *et al.*, J. Phys. Chem. **89**, 4501 (1985).

[67] M. F. Golde, Y.-S. Ho. and H. Ogura, J. Chem. Phys., **76**, 3535 (1982).

[68] N. A. Khromov, Candidate Thesis [in Russian], SPbU, St. Petersburg, 1991.

[69] H. Hotop, E. Kolb, and J. Lorenzen, J. Electron. Spectrosc. **16**, 213 (1979).

[70] K. Ohno, H. Mutoh, and Y. Harada, J. A. Chem. Soc. **105**, 4555 (1983).

[71] E. E. Ivanov, Yu. Z. Ionikh, N. P. Penkin *et al.*, KhVE, **18**, 159 (1984).

[72] L. D. Landau and E. M. Lifshitz, *Quantum Mechanics*, Pergamon Press, Oxford, 1965 [Russ. original, Fizmatgiz., M., 1963].

[73] G. J. Schulz, Rev. Mod. Phys. **45**, 378 (1973).

[74] L. A. Vaĭnshteĭn and L. A. Minaeva, Zh. Prikl. Spektrosk. **9**, 60 (1968).

[75] R. K. Nesbet, Phys. Rev. A **12**, 444 (1975).

[76] M. Schaper and H. Scheibner, Beitr. Plasmaphys. **9**, 45 (1969).

[77] A. I. Korotkov, L. K. Mitryukhin,, N. A. Prilezhaeva *et al.*, *Abstracts of Papers Read to the Eighth All-Union Conference on the Physics of Electron and Atomic Collisions* [in Russian], 1981, p. 199 (LIYaF Preprint).

[78] F. M. J. Pichanik and J. A. Simpson, Phys. Rev. **168**, 64 (1968).

[79] J. N. H. Brunt, G. C. King, and F. H. Read, J. Phys. B. **9**, 2195 (1976).

[80] J. N. H. Brunt, G. C. King, and F. H. Read, J. Phys. B. **10**, 3781 (1977).

[81] A. A. Zavilopulo, A. V. Snegurskiĭ, O. B. Shpenik *et al.*, Zh. Eksp. Teor. Fiz. **81**, 842 (1981) [Sov. Phys. JETP **54**, 449 (1981)].

[82] J. M. Phylips, J. Phys. B **15**, 4259 (1982).

[83] N. B. Kolokolov, R. I. Lyagushchenko, and P. M. Paramatarov, Zh. Tekh. Fiz. **47**, 2108 (1977) [Sov. Phys. Tech. Phys. **22**, 1225 (1977)].

[84] R. Deloche, P. Monchicourt, M. Cheret *et al.*, Phys. Rev. A **13**, 1140 (1976).

[85] W. E. Wells, P. Monchicourt, R. Deloche *et al.*, J. Phys. **34**, 381 (1973).

[86] N. B. Kolokolov, A. A. Kudryavtsev, and V. A. Romanenko, Zh. Tekh. Fiz. **58**, 2098 (1988) [Sov. Phys. Tech. Phys. **33**, 1274 (1988)].

[87] D. R. Bates, K. L. Bell, and A. E. Kingston, Proc. Phys. Soc. London **91**, 288 (1967).

[88] G. J. Schulz and R. E. Fox, Phys. Rev. **106**, 1179 (1957).

[89] I. Ya. Fugol', O. N. Grigorashchenko, and D. A. Myshkis, Zh. Eksp. Teor. Fiz. **60**, 423 (1971) [Sov. Phys. JETP **33**, 227 (1971)].

[90] G. N. Gerasimov, G. P. Startsev, and M. S. Frish, Opt. Spektrosk. **32**, 1032 (1972).

[91] L. A. Vaĭnshteĭn, I. I. Sobel'man, and E. A. Yukov, *Cross Sections for the Excitation of Atoms and Ions by Electrons* [in Russian], Nauka, M., 1973.

[92] D. S. Newman, M. Zubek, and G. C. King, J. Phys. B **18**, 185 (1985).

[93] W. L. Borst, Phys. Rev. **181**, 257 (1969).

[94] B. L. Moiseiwitsch and S. J. Smith, Rev. Mod. Phys. **40**, 238 (1968).

[95] V. I. Demidov and N. B. Kolokolov, Zh. Tekh. Fiz. **50**, 564 (1980) [Sov. Phys. Tech. Phys. **25**, 338 (1980)].

[96] V. I. Demidov and N. B. Kolokolov, Phys. Lett. A **89**, 397 (1982).

[97] A. P. Zhilinskiĭ, I. F. Liventsova, and L. D. Tsendin, Zh. Tekh. Fiz. **47**, 304 (1977) [Sov. Phys. Tech. Phys. **22**, 177 (1977)].

[98] V. I. Demidov, N. B. Kolokolov, and O. G. Toronov, Fiz. Plazmy **12**, 702 (1986) [Sov. J. Plasma Phys. **12**, 402 (1986)].

Translated by S. Chomet